8

ANTENNAS AND RF COMMUNICATION

Asimina Kiourti and Konstantina S. Nikita

School of Electrical and Computer Engineering, National Technical University of Athens, Athens, Greece

8.1 INTRODUCTION

Wireless biomedical telemetry systems performing in the RF bands attract significant scientific interest due to their promising applications in the field of patient care inside hospital, home, or even outside environments. The major drawback of historically reported biomedical telemetry systems was the wired communication between the medical devices and an exterior monitoring/control equipment, which significantly limited patient comfort and convenience. Therefore, biomedical telemetry devices with wireless communication functionalities appear as a highly promising option toward improving the patients' quality of life and providing medical systems with constant availability, context awareness, reconfigurability, and unobrusiveness (Jovanov et al., 2003). Nowadays, RF biomedical telemetry systems are further facilitated by the continuously increasing advancements in wireless communications, standards, and components.

Wireless medical devices and, thus, antennas integrated into them can be divided into three categories, according to their placement on or inside the patient's body: (1) on-body, (2) implantable, and (3) ingestible antennas.

Handbook of Biomedical Telemetry, First Edition. Edited by Konstantina S. Nikita.

1. *On-body antennas* are intended to be placed on the human body or be worn as part of an individual's garment. In the first case, antennas are designed and meant to be integrated on medical devices that are placed on the patient's body. In the second case, antennas are designed to form part of the patient's clothing, thus, attempting to enhance the functionalities of everyday clothing. Optimal integration of a wearable antenna into clothing can be achieved by making the antenna itself out of a conductive and smart textile material. Example on-body medical devices include temperature monitors, accelerometers, pulse oximeters, electromyogram sensors, and the like.
2. *Implantable antennas* are intended for integration into medical devices that will be implanted inside the human body by means of a surgical operation. Epidermal as well as deep implantation of the medical device are included in this category. Millions of people worldwide depend upon implantable medical devices to support and improve the quality of their lives. Wireless medical implants are already in use for a wide variety of applications such as temperature monitors, pacemakers, functional electrical stimulators, cochlear and retinal implants, and the like. As technology continues to evolve, their use is expected to rapidly increase from an already large base.
3. *Ingestible antennas* are intended for integration into medical devices that have the form of a capsule to be swallowed and ingested by the patient. Wireless capsule endoscopy receives considerable attention for diagnosing diseases of the gastrointestinal (GI) tract. The purpose is for the capsule to be swallowed and wirelessly transmit images and video outside the body. Ideally, wireless transmission will be performed in real time, while the capsule travels along the GI tract.

   Regardless of their positioning, the utmost aim of on-body, implantable, and ingestible devices is to improve the patients' quality of life by providing them with convenient and continuous monitoring systems. Ever growing miniaturization of antennas along with the recent advancements in electronics components and information and communication technologies (ICTs) promise the development of a wide variety of miniature medical devices that can be worn by, implanted into, or ingested by a patient without causing any sort of discomfort.

Before the widespread use of on-body, implantable, and ingestible antennas, however, there are a number of technical challenges that need to be addressed, mainly in terms of design and channel modeling. Antennas are essential parts of RF biomedical telemetry systems, with their complexity highly depending on the surrounding tissue environment (proximity to the human body), and the electronics, communications, and medical requirements. For example, such antennas are required to be small, lightweight, robust, conformal to the body surface, and biocompatible, yet maintaining an improved radiation and patient safety performance. An overview of these challenges is outlined below for on-body, implantable, and ingestible antennas, along with solutions proposed so far in the literature.

8.2 BACKGROUND INFORMATION

An antenna can be defined as the transitional structure between free space and a guiding device (coaxial line or waveguide), which is used to transport electromagnetic energy from the transmitting source to the antenna or from the antenna to the receiver. In addition to transmitting or receiving energy, an antenna in an advanced wireless system is usually required to optimize or accentuate the radiation energy in some directions and suppress it in others. Thus, the antenna must also serve as a directional device in addition to a probing device.

To describe the performance of an antenna, definitions of various parameters are necessary (Balanis, 2002):

- An *antenna radiation pattern* is defined as a mathematical function or a graphical representation of the radiation properties of the antenna as a function of space coordinates. Radiation properties may include power flux, density, radiation intensity, and the like. In most cases, the radiation pattern is determined in the far-field region and is represented as a function of the directional coordinates.
- The space surrounding an antenna is usually sub-divided into three regions. The *reactive near-field region* is the portion of the near field where the reactive field predominates and is commonly taken to exist at a distance $R < 0.62\sqrt{D^3/\lambda}$, where λ is the wavelength and D is the largest dimension of the antenna. The *radiating near-field (Fresnel) region* is the region wherein radiation fields predominate and wherein the angular field distribution depends upon the distance from the antenna. The outer boundary is taken to be $R < 2D^2/\lambda$. Finally, the *far-field (Fraunhofer) region* is defined as the region where the angular field distribution is essentially independent of the distance from the antenna and is commonly taken to exist at distances greater than $2D^2/\lambda$ from the antenna.
- *Directivity* of an antenna is defined as the ratio of the radiation intensity in a given direction from the antenna to the radiation intensity averaged over all directions. On the other hand, the *gain* of an antenna is defined as the ratio of the intensity, in a given direction, to the radiation intensity that would be obtained if the power accepted by the antenna was radiated isotropically. Therefore, an antenna's directivity is a component of its gain.
- *Input impedance* is defined as the impedance presented by an antenna at its terminals or the ratio of the voltage to current at a pair of terminals or the ratio of the appropriate components of the electric to magnetic fields at a point.
- The *reflection coefficient* of an antenna is defined as the ratio of the reflected waves' amplitude to the amplitude of the incident wave. The reflection coefficient is zero if the transmission line impedance is the complex conjugate of the antenna impedance.
- Finally, the *bandwidth* of an antenna is defined as the range of frequencies, on either side of a center frequency, within which the performance of the antenna (e.g., input impedance, reflection coefficient, etc.) is within an acceptable value of that at the center frequency.

8.3 ON-BODY ANTENNAS

8.3.1 Antenna Design

There exist several challenges regarding the design of on-body antennas, as summarized below. Research on on-body antennas attracts growing interest in both academia and industry, and many efforts have been reported in the literature toward the design of on-body antennas for communication with exterior antennas or even other on-body antennas. It is important to highlight that even though these challenges are more or less common for most on-body antennas, precise requirements on the antenna design should, in each case, be determined by the designer given the medical application in hand.

Selection of Operation Frequency In the United States, the Federal Communications Commission (FCC) has allocated the bands of 608–614, 1395–1400, and 1427–1432 MHz for wireless medical telemetry service (WMTS), as well as the bands of 902–928 and 2400.0–2483.5 MHz for industrial, scientific, and medical (ISM) applications. In Europe, the frequency bands of 433.1–434.8 and 868.0–868.6 MHz are used for ISM applications, and they are defined by the Electronic Communications Committee (ECC). Finally, the Ultrawide Band (UWB) of 3.1–10.6 GHz, which has been authorized by the FCC, receives considerable attention because of the wide bandwidth offered.

Type and Material of the Antenna Microstrip and loop designs are generally applied for on-body antennas because of their conformability and light weight. However, for several on-body links (i.e., links formed between on-body antennas placed on the patient's body), and for many body postures, quarter-wavelength ($\lambda/4$) monopole antennas placed on a small ground plane have been shown to perform even better. The main reason is that the monopole antenna exhibits an omnidirectional radiation pattern, which is highly preferable in cases where the geometry and the characteristics of the wireless link are unknown. On the other hand, in certain medical application and posture scenarios, directive planar inverted-F antenna (PIFA) geometries placed so that the direction of maximum radiation is oriented toward the direction of the receiving antenna have been shown to achieve reduced loss in the wireless link as compared to that achieved by monopole antennas.

Miniature coplanar waveguide (CPW)–fed tapered slot antennas (TSA), as well as planar inverted cone antennas (PICA) have also been reported for UWB biomedical telemetry (Alomainy et al., 2009) (Figure 8.1). Both antennas were proved to meet the UWB requirements with regards to impedance, radiation bandwidth, and impulse responses (pulse fidelity) with average fidelity of 86 and 88% for TSA and PICA, respectively. Unlike the conventional wide-band CPW-fed antenna (Chen, 2005), the TSA employed two diverging tapered slots to provide better impedance matching between 3.1 and 10.6 GHz. The TSA antenna did not show any strong resonance within the band and hence exhibited less group delay variation. Furthermore, its radiation was found to be more directive, thus making it resilient to variations in the tissue and surrounding indoor/outdoor environment.

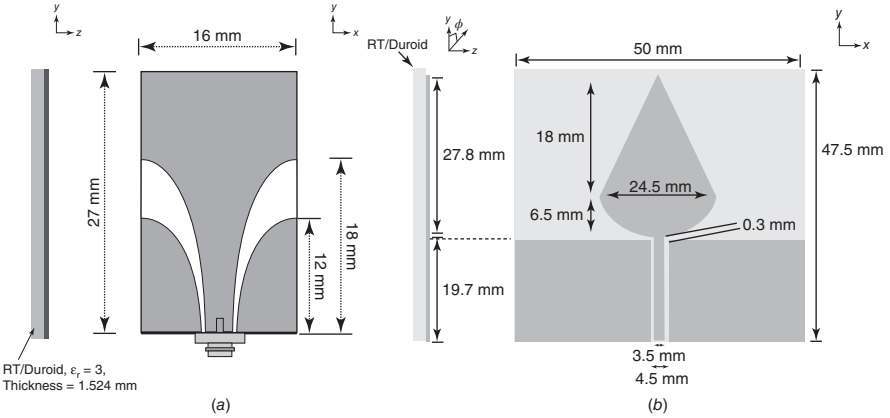

Figure 8.1 Geometry of (*a*) TSA and (*b*) PICA proposed for on-body medical telemetry applications (Alomainy et al., 2009).

In terms of material, the aim should be for the antenna structure to be easy to attach to the body or clothing, without the selected material restricting its possible placements onto the body. Practically, there is no limitation for the material of antennas that are intended for integration into on-body medical devices. However, despite having the potential to be relatively inexpensive, such antennas may be inflexible and high profile. For this purpose, textile antennas with the ability to be attached into everyday clothing are studied. Conductive textile materials, known as electrotextiles (e-textiles), which can function as electronics while physically behaving as textiles, enable the fabrication of textile antennas (Klemm et al., 2004). Both electrical properties (e.g., conductivity) and mechanical properties (e.g., flexibility) are crucial in the fabrication of e-textiles. The methods most commonly used to integrate conductivity into textiles include stitching, weaving, knitting, and printing.

For example, a UWB antenna made from textile materials has been presented (Osman, et al., 2011). The antenna was characterized as a "fully textile" antenna because textiles were used for both its substrate and its conducting parts. The antenna exhibited a wide, 17 GHz of bandwidth, omnidirectional patterns and adequate gain and efficiency values, and was found to meet the requirements of robustness, low power consumption, and compactness. Experimental investigations were carried out, and measurement results were compared with simulations, indicating good agreement.

A weakness of most planar textile antennas proposed in the literature is that they require a coaxial cable to be connected to the transceiver (Tronquo et al., 2006). Such a feeding technique is rigid, and, thus, relatively disturbing to the patient wearing the antenna. To meet this requirement and overcome such difficulties with feeding structures, the coaxial cable feed can be replaced by a microstrip feed line, which couples its power into the antenna through an aperture in the ground plane. The first aperture-coupled patch antenna (ACPA) made of textile materials has been presented in Hertleer et al. (2007) (Figure 8.2). The result was a highly efficient, fully flexible

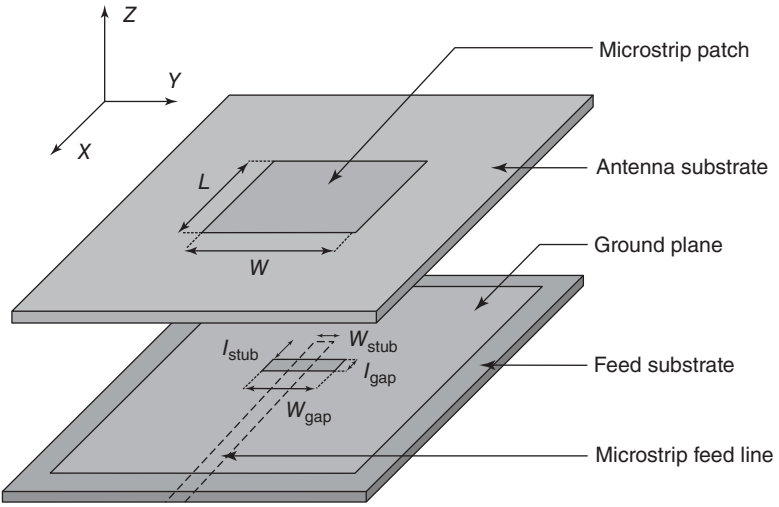

Figure 8.2 Geometry of an ACPA proposed for integration into wearable textile systems (Hertleer et al., 2007).

antenna, that was easy to integrate into garments for wireless medical telemetry in the 2.45 GHz ISM band.

Influence of Human Body Performance of on-body antennas is considerably affected by their close proximity to human tissues. Commonly reported issues include antenna detuning (shift of the resonance frequency and change in the input impedance of the antenna), distortion of the radiation pattern, and degradation of the radiation efficiency (Scanlon and Evans, 2001; Okoniewski and Stuchly, 1996; Wong and Lin, 2005). To get a deeper understanding of the way that on-body antennas interact with the human tissues, it becomes necessary to investigate the performance of such antennas when they are mounted close to the body.

For example, experimental investigations inside a reverberation chamber for five compact on-body antennas operating at 2.45 GHz and worn by nine individual test subjects have shown standard deviations of the antenna radiation efficiency of less than 0.6 dB and resonance frequency shifts of less than 1% (Conway et al., 2008). Such variabilities were found to significantly depend on body tissue coupling, which is, in turn, related to the antenna geometry and radiation characteristics. Even though the test subjects were asked to remain stationary, the measured results included all natural body movements. Further measurements carried out in tissue-emulating phantoms rather than in live subjects demonstrated the suitability of phantoms for assessing the performance of on-body antenna configurations.

For medical applications, antennas need to be immune from frequency detuning. For this purpose, wide-band designs need to be targeted for on-body antennas. At this point, it is important to highlight that, unlike its narrow-band counterpart, the design of a UWB antenna is determined not only by its reflection coefficient characteristics

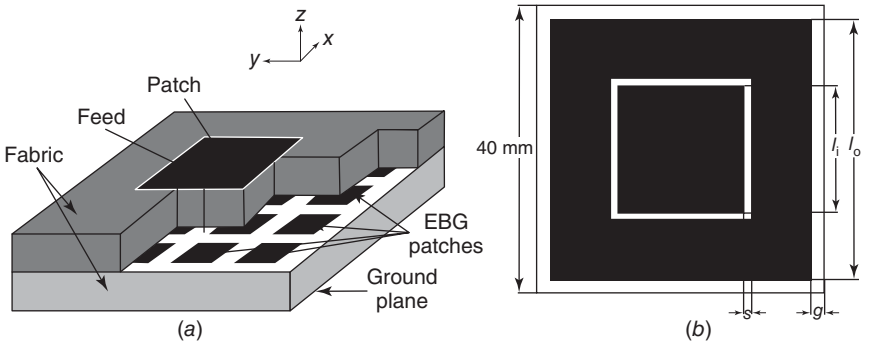

Figure 8.3 Geometry of (*a*) wearable electromagnetic band gap antenna (WEBGA) (Salonen et al., 2004a) and (*b*) dual-band coplanar antenna on EBG substrate (Zhu and Langley, 2009) proposed for overcoming the radiation into the human body.

but also by its ability to preserve the pulse shape. As a result, antennas for UWB systems are required to have very broad impedance bandwidth, as well as stable and constant channel transfer response and high efficiency.

Furthermore, understanding the influence of the human body on the antenna radiation pattern becomes vital in determining its actual radiation performance (Scanlon and Evans, 2001; Chen, 2007). The technique of designing on-body antennas on electromagnetic band gap (EBG) substrates has been reported for overcoming the radiation absorption inside the human body and achieving higher values of antenna gain. Example antennas are shown in Figure 8.3 (Salonen et al., 2004a; Zhu and Langley, 2009). Another reported solution is the design of highly directive antennas that are not affected from the reflections of the human body, such as the miniature TSA UWB antenna proposed in Alomainy et al. (2009) (Figure 8.1*a*).

Multi-band Operation On-body antennas most commonly focus on single-frequency operation. However, there exists an increased demand on multi-frequency or, equivalently, multi-functional on-body antennas. In other words, the antenna is required to operate at different frequencies in order to perform more than one task at the same time, thus accounting for new technologies and services available to the patient/user.

For example, a dual-band wearable textile antenna has been reported for simultaneous operation at 1900 [Global System for Mobile Communications (GSM)] and 2400 MHz [wireless local area network (WLAN) and ISM] (Salonen, et al., 2004b). The antenna had a U-shaped slot structure mounted on the surface of fleece fabric, which enabled the antenna to be flexible, low profile, and lightweight (Figure 8.4*a*). In this study, the antenna was fabricated and measured, with good agreement being observed between measurements and simulations (Figure 8.4*b*).

Effect of Surrounding Electronics Components Design of on-body antennas is most commonly performed by ignoring the structure of the medical device into which the antenna is to be integrated. This involves the surrounding circuitry of the medical

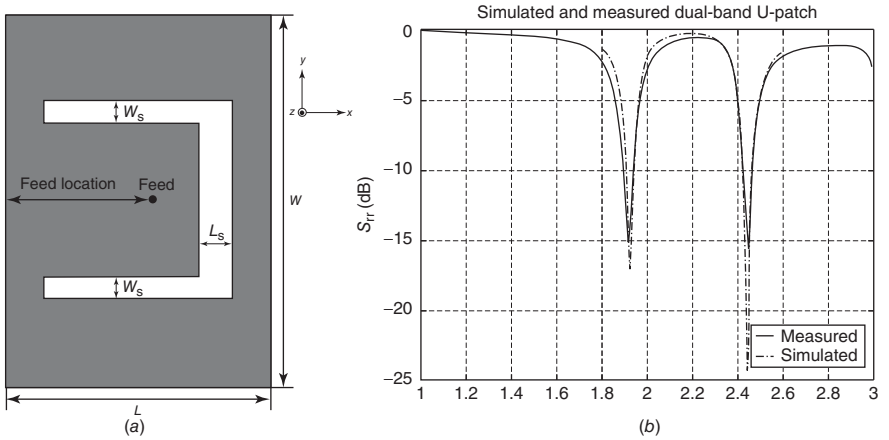

Figure 8.4 (*a*) Geometry of a dual-band wearable textile antenna and (*b*) simulated and measured reflection coefficient frequency response (Salonen et al., 2004b).

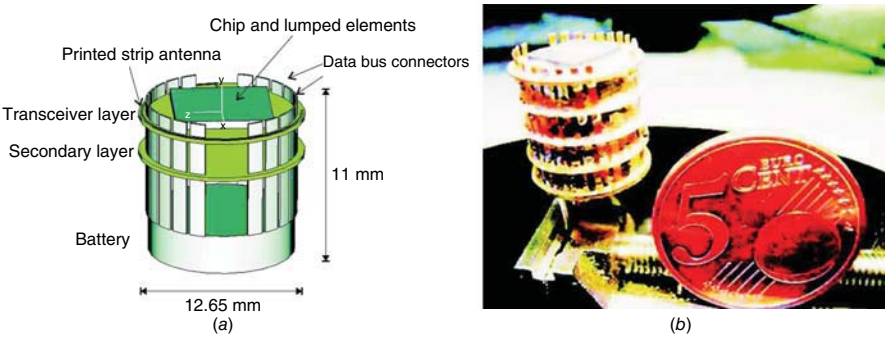

Figure 8.5 (*a*) Schematic of the sensor used in numerical analyses and (*b*) picture of the fabricated sensor used in experimental investigations to assess the effect of the surrounding components on the performance of an on-body antenna (Alomainy et al., 2007a).

device, including integrated circuits (ICs) and lumped elements. However, antenna operation and performance are expected to vary according to those parameters that govern the operation of the overall medical device.

To address this issue, a study has been performed that illustrated the importance of including the details of the medical device in determining and analyzing the performance of an on-body antenna (Alomainy et al., 2007a). The overall sensor structure was designed for operation in the 2.4-GHz band, and was compact enough to address the miniaturization requirements of medical devices. A schematic of the sensor structure applied in the numerical analysis, as well as a picture of the fabricated prototype sensor are shown in Figure 8.5. Table 8.1 compares the antenna gain, radiation, and total efficiency of a printed monopole antenna designed in free space to that of a sensor-matched printed monopole antenna. As compared to a conventional printed

TABLE 8.1 Comparison of Stand-Alone and Sensor-Matched Printed Monopole Antennas (Alomainy et al., 2007a)

Antenna	Gain (dBi)	Radiation Efficiency (%)	Total Efficiency (%)
Stand-alone monopole	−1.2	48	2
Sensor-matched monopole	1.6	77	75

antenna, an antenna that had been optimized for a specific sensor design demonstrated an increase in gain by 2.8 dB, an improvement in radiation efficiency by 29%, and an enhancement in the sensor coverage area by 25%. Limitations related to the placement of the components around the antenna were found to be highly challenging in determining and improving its performance in terms of impedance matching, gain, efficiency, and front-to-back ratio of the radiated energy.

Antenna Diversity The requirements of high data rate and reliable data transmission between on-body medical devices and exterior equipment or between on-body medical devices themselves necessitate the use of multiple antennas. Antenna diversity is a technique where two or more signals from several independent and, thus, uncorrelated diversity branches are combined in different ways to form a unique signal, known as the diversity combined signal. This technique can be accomplished in a number of ways. It may involve the use of different antennas (space diversity), different radiation patterns (pattern diversity), or different polarizations (polarization diversity). Space diversity is achieved by using more than one antenna at the transmitter or receiver side and is by far the most popular technique. For example, a space diversity monopole antenna with variable spacing d is shown in Figure 8.6a (Khan et al., 2009). Pattern diversity is achieved by using different radiation patterns in the same or separate antenna. Finally, polarization diversity is achieved by using a single antenna with multiple polarizations or separate antennas with different polarizations.

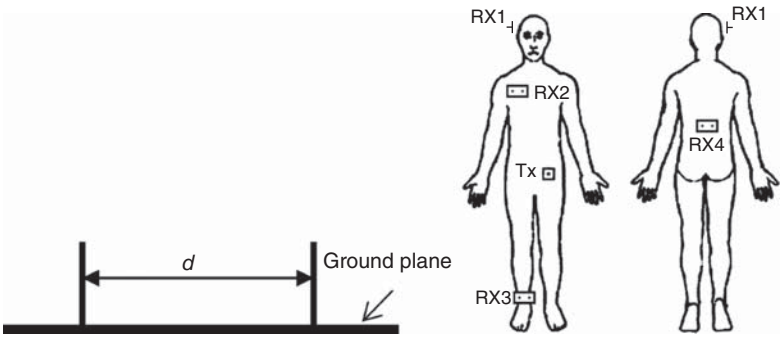

Figure 8.6 (*a*) Space diversity monopole antenna with variable spacing (Khan et al., 2009), and (*b*) analyzed positions for diversity antennas (Serra et al., 2007).

The aim of antenna diversity is to overcome channel fading and provide an efficient link in terms of power. It should be noted that, in the case of on-body channels, fading may occur due to the relative movement of the body parts, shadowing, polarization mismatch, and scattering due to the body and surrounding environment. Use of diversity removes the deep fades, thus decreasing the rate of crossing and the duration of the lower fade levels for the resultant combined signal.

The improvement offered by the diversity technique is most commonly quantified in terms of the diversity gain (DG). Diversity gain is defined as the improvement in the signal-to-noise ratio (SNR) or the bit error rate (BER) over a single antenna with no diversity at some level of outage probability, and strongly depends on the correlation and power imbalance among the signals of the diversity branches. However, second-order statistics can also be used to quantify the results of applying the diversity technique.

Preliminary diversity measurements with monopole antennas at 2.45 GHz have shown that antenna diversity can offer significant improvement for the on-body channels, that is, the channels formed between medical devices placed onto a patient's body. For example, in Serra et al., (2007) a monopole antenna was used as a transmitter (Tx), and two monopoles on a common ground plane were used as a receiver (Rx). Antenna locations under study are shown in Figure 8.6*b*. Measurements were carried out in an anechoic chamber in order to solely assess the scattering and fading effects of the body itself. Table 8.2 summarizes measured diversity gain results at 99% reliability levels. Different combining techniques [selection combining (SC), equal-gain combining (EGC), and maximum ratio combining (MRC)] have been considered for comparison purposes. In Khan et al. (2009), three different types of 2.45-GHz antennas were considered for five body channels, and measurements were taken in anechoic and indoor environments. High diversity gains achieved suggested that multipath is noticeable in the on-body propagation channels. In this study, the PIFA was shown to be the best choice of antenna, exhibiting reasonable path gains and high diversity gains.

Diversity analysis for on-body channels at 5.8 and 10 GHz has also been performed, by using different types of antennas for space and pattern diversity (Khan and Hall, 2009). Same as for the 2.4-GHz case, the PIFA was proved to be the best choice of antenna for the deployment of the diversity technique. The 5.8-GHz frequency was shown to be the best choice in terms of cost (hardware cost and complexity at 10 GHz are higher than those at 5.8 GHz) and path loss (path loss at 5.8 GHz was found to be

TABLE 8.2 Diversity Gain for Antenna Placements Indicated in Figure 8.6*b*

	Standing				Sitting		Jogging	
DG	Rx3	Rx1	Rx2	Rx4	Rx2	Rx4	Rx3	Rx1
SC	2.57	4.61	2.17	5.86	3.10	0.79	5.14	8.57
EGC	3.69	5.53	3.16	6.65	3.29	2.44	6.13	9.62
MRC	4.28	6.00	3.89	7.12	4.22	2.90	6.46	10.28

Source: Serra et al. (2007).

less than that at 10 GHz). Positioning and orientation of the diversity antennas were found to introduce minor discrepancies.

8.3.2 Channel Modeling

Two communication channels can be considered for on-body medical devices:

(a) *On-body channels* refer to the wireless communication between on-body medical devices. Such channels involve transmission paths on the body as well as paths scattering off the local environment of the body (indoors or outdoors).
(b) *Off-body channels* refer to the wireless communication between an on-body medical device and an exterior/remote device and deal with electromagnetic wave propagation around the body.

For example, in the case of a biomedical telemetry application where on-body medical devices communicate with a wearable device, both on- and off-body propagation channels need to be considered. In this case, the wearable device may act as a controller that relays data between the on-body devices and remote stations.

Radiowave propagation in on-body and off-body channels is much more complicated as compared to propagation between two antennas placed in free space, for example, between a cellular phone and a cellular base station. The first reason is the dynamic nature of the human body. During normal activity, movements of the human body can be significant or, in certain cases (e.g., sports), extreme. Even when standing or sitting, the human body is subject to several small movements. As a result, the characteristics of the wireless link and, hence, system performance change rapidly. Furthermore, the human body is a complex problem to be solved numerically, as attributed to variations in anatomy and dielectric properties between individuals, as well as varying dielectric properties of tissues with frequency. In terms of numerical simulations, the body is a rather large problem, which can be considered to be at the edge of what can currently be managed on single-PC-based solvers and requires the use of cluster computing. The need for accurate simulation of the body's postures and movements is also highly challenging.

In order to enable the design of reliable and robust communication links for on-body medical devices, it becomes necessary to develop deterministic and generic channel models. The aim is to provide a clear picture of the propagation channel and its behavior with regard to different body dynamics and exterior environments. Given that there already exist models for indoor and outdoor propagation, it becomes crucial to combine the on-body propagation models with existing environmental models or statistics in order to get the full picture. In any case, during channel characterization, there are difficulties in de-embedding the antenna characteristics from those of the propagation path or, equivalently, separating the performance of the antenna from the channel characteristics.

There have been a number of research studies that aim to characterize and analyze the on- and off-body channels. Results for various transmitter and receiver antenna

combinations over various on- and off-body paths have been presented at 2.45 GHz as well as in the UWB, as outlined below.

Studies at 2.45 GHz Measurements of path loss for several on-body antenna locations at 2.45 GHz have been carried out in Hall et al. (2007). Transmitter or receiver locations are shown in Figure 8.7*a*, while measurements were performed both in an anechoic chamber and in other surroundings. Monopoles over a small ground plane were chosen because of their omnidirectional radiation pattern, which rendered the results independent of antenna orientation. Variability in path loss due to different antenna placement and changes in posture was found to be as much as 50 dB. Example path gain variations are shown in Figure 8.7*b*. In Figure 8.7*c*, path gain values are plotted as a function of the separation between the antennas measured along the shortest geodesic path around the body. The path gain of antennas in free space, as given by the Friis formula, is shown in solid line. Data points for line-of-sight (LOS) propagation

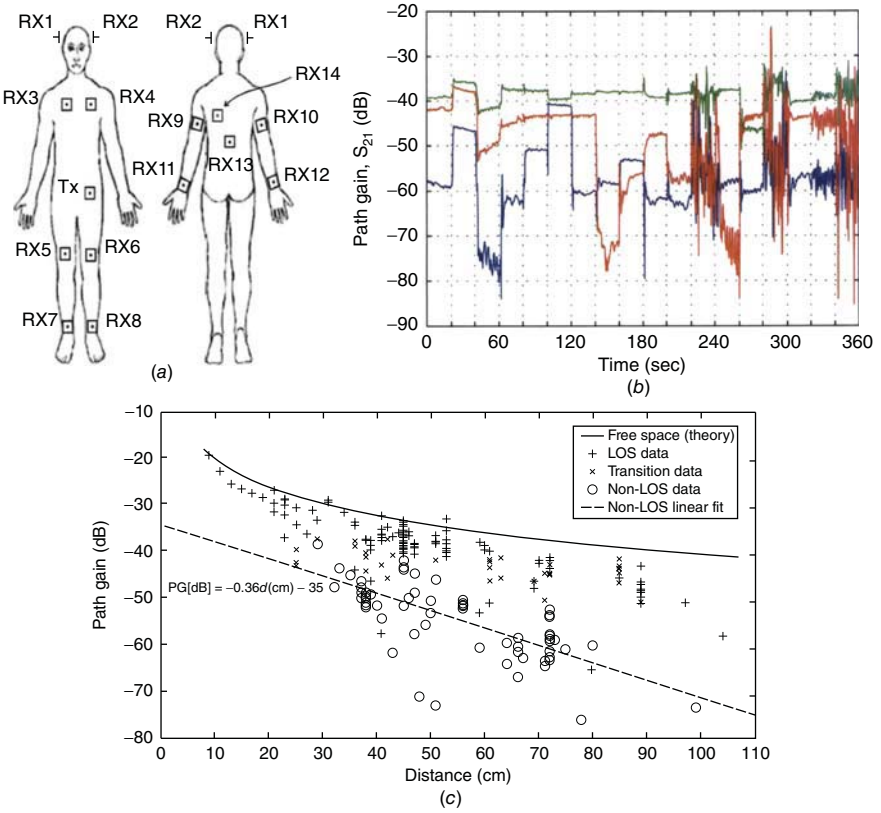

Figure 8.7 (*a*) Possible transceiver locations on the body, (*b*) measured path gain variations for Rx1 (blue), Rx3 (green), and Rx12 (red) and, (c) path gain as a function of the separation between the antennas measured along the shortest geodesic path around the body. (*See insert for color representation of b.*)

scenarios are denoted by +. Most of the LOS data followed the free-space curve with a mean difference between the measured and theoretical values of − 5.1 dB. Thus, the path gain in LOS scenarios was said to be given by

$$G_P\,(\text{dB}) = -5.33 - 20\log_{10} d \tag{8.1}$$

where d is the distance between the antennas in centimeters.

Non-line-of-sight (NLOS) data points are denoted by ○, and were also shown to follow a trend corresponding to an exponential attenuation, according to

$$G_P\,(\text{dB}) = -0.36d - 35 \tag{8.2}$$

Propagation scenarios that could not be identified as LOS or NLOS are shown by × marks. Some of them seemed to follow the same trend as the LOS data points, while others were clustered together with the NLOS data points.

Given the high number of communication paths and their variability associated with different postures, no single channel model was shown to be satisfactory. A classification of body postures based on their spatial and temporal characteristics was rather suggested for future research.

The coupling performance of patch antennas placed in close proximity to a lossy medium that simulated body tissues has further been studied (Conway and Scanlon, 2009). The performance of higher mode microstrip patch antennas (HMMPA) was evaluated both numerically and experimentally and further compared with that of a microstrip patch excited at its fundamental mode (MPA-F) and a fundamental microstrip patch antenna with the addition of a shortening wall (MPA-S). Significant channel fading was recorded during normal activity, as attributed to the dynamic nature of the human body and the surrounding multipath.

Statistical analyses for on-body radio propagation channels have also been performed. Channel measurements using two microstrip patch antennas for a range of body positions and postures were presented and statistically analyzed in Alomainy et al. (2007b). Attenuation attributed to factors such as the body, head, and clothing was estimated as 19.2, 13.0, and 1.7 dB, whereas the measured cumulative distribution function of the data was found to fit to the log-normal distribution. An effort toward gathering and statistically analyzing a large amount of data in practical environments (inside and outside an office block, in the home, while driving) has been performed in Hu et al. (2007). The measured variations in path loss appeared to be nonstationary, thus leading to multimodal probability distributions, which could not be represented by a simple theoretical formula. However, an approximate fit to one of standard probability distributions was found to be achieved by limiting the number of data samples.

Studies in UWB Given the frequency dependency of the dielectric properties of human tissues, characterization of the UWB on-body channels appears to be more challenging than that of the narrow-band channels. The conventional and empirical models available for many narrow-band and wide-band systems are insufficient to describe the UWB channel.

An initial characterization of the UWB on-body channel was presented in Zasowski et al. (2003). A predefined set of nodes with multi-hopping networking was considered in order to determine the energy and power requirements. However, realistic behaviors of the human body, such as different body postures and movements, were not analyzed.

A detailed description of the measurement procedure performed to obtain sufficient path loss data for acceptable characterization of UWB on-body channels has appeared in Alomainy et al. (2005). The performance of horn-shaped self-complementary (HSCA) and PICA antennas was analyzed. Results showed that the hybrid use of different types of UWB antennas could effectively improve channel behavior. As compared to the PICA, the HSCA exhibited reduced values of the mean RMS delay spread for cases where surface waves were dominant in the wave traveling along the human body. Path loss analysis demonstrated NLOS behavior as attributed to attenuation and shadowing by the human body.

Free-space and body-mounted characterization of UWB CPW-fed TSAs and inverted cone antennas (PICAs) was performed in Sani et al. (2010). Results demonstrated that the Nakagami model provided the best fit to the root mean square (RMS) delay spread. If a more omnidirectional antenna (PICA) was used, the goodness of the statistical model became lower, whereas the time delay behavior was degraded. Using a less sensitive receiver, the statistical model was proved to be more deterministic.

Investigations on the effect of body movements on the UWB radio channel have also been performed. An experimental investigation to derive suitable radio propagation models for UWB channels of on-body medical devices was carried out in Abbasi, et al. (2010). Measurements were performed for 35 radio links, considering both stationary and pseudodynamic movements of the human body, and radio channel parameters were extracted and statistically analyzed to provide a radio propagation model with the inclusion of pseudodynamic body motion effects. For the static and pseudodynamic motion scenarios, less than 25 and 30% of the on-body links demonstrated bad link quality, respectively. The upper and lower parts of the body were shown to provide relatively stable radio channels. Another measurement campaign with the subject performing movements of different nature in order to cover a wide range of scenarios and ensure sufficient data collection for statistical analysis was presented in Abbasi et al. (2011a). Four links were targeted (belt to head, belt to chest, belt to wrist, and belt to ankle), and measurements were performed inside an anechoic chamber and indoor environments. The normal distribution was found to provide the best fitting for the path loss, while the RMS delays were better modeled with a log-normal distribution.

Finally, investigations on potential power-efficient UWB orthogonal frequency division multiplexing-based channels (UWB-OFDM) for on-body medical devices have been carried out (Abbasi et al., 2011b). The BER performance of the system under study showed that the lower part of the body for the on-body channels and the lower part of the trunk for the off-body channels provided relatively stable radio channels with a good-quality link.

In terms of modeling, the ray tracing (RT) technique and the finite-difference time-domain (FDTD) method have been widely applied to propagation modeling for UWB systems. For example, a simulation model for UWB indoor radio channels using RT has been proposed in Attiya (2004). The FDTD method has been applied to characterize the UWB radio channel for the chest-to-waist link (Wang and Wang, 2009) and simulate pulse propagation around the torso at 2–6 GHz (Fort, 2005). A deterministic on-body channel model using a subband FDTD method was suggested in Zhao et al. (2006). Numerical results were compared to those from a hybrid uniform geometrical theory of diffraction (UTD)/RT model, demonstrating the ability of the proposed method to model materials with any frequency dependence and deal with complicated on-body radio channels.

8.4 IMPLANTABLE ANTENNAS

8.4.1 Antenna Design

A key and critical component of wireless implantable medical devices is the integrated implantable antenna that enables its bidirectional communication with exterior monitoring/control equipment. Design of implantable antennas is highly intriguing, with the main challenges being outlined below (Kiourti and Nikita, 2012a).

Selection of Operation Frequency A few years ago no globally accepted frequency band had been dedicated for biomedical telemetry of implantable medical devices. The situation changed with the International Telecommunications Union—Radiocommunications Recommendation SA.1346 (ITU-R, 1998), which outlined the use of the 402–405 MHz frequency band for Medical Implant Communications Systems (MICS). The 433.1–434.8 MHz, 868–868.6 MHz, 902.8–928 MHz, and 2400–2500 MHz ISM bands are also suggested for biomedical telemetry of medical implants. However, focus is on the MICS band because of its advantages to be available worldwide and feasible with low-power and low-cost circuits, reliably support high data rate transmissions, fall within a relatively low noise portion of the spectrum, lend itself to small antenna designs, and propagate acceptably through human tissue.

Type and Material of Antenna Patch designs are mostly preferred for implantable antennas because they are highly flexible in design and conformability. In a realistic scenario, the implantable patch antenna will be mounted on the existing hardware of the medical implant, which will also serve as its ground plane.

Implantable antennas must be biocompatible in order to preserve patient safety and prevent rejection of the implant. Furthermore, human tissues are conductive and would short-circuit the implantable antenna if they were allowed to be in direct contact with its metallization. To preserve biocompatibility, while at the same time separating the metal radiator from human tissue, the most widely used approach is to cover the structure by a superstrate dielectric layer (Figure 8.8a). Commonly used biocompatible materials include Teflon (permittivity, $\varepsilon_r = 2.1$, dielectric loss tangent,

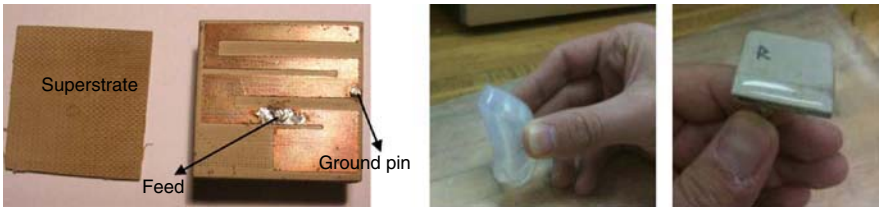

Figure 8.8 Biocompatibility issues for implantable antennas: (*a*) addition of a superstrate (Karacolak et al., 2009) and (*b*) thin-layer encapsulation (Karacolak et al., 2010).

tan $\delta = 0.001$), MACOR ($\varepsilon_r = 6.1$, tan $\delta = 0.005$), and ceramic alumina ($\varepsilon_r = 9.4$, tan $\delta = 0.006$) (Soontornpipit et al., 2004). Insulating the implantable antenna with a thin layer of low-loss biocompatible coating is another reported approach (Figure 8.8*b*). Materials proposed for biocompatible encapsulation include zirconia ($\varepsilon_r = 29$, tan $\delta \approx 0$) (Skrivervik, 2011), polyether ether betone (PEEK) ($\varepsilon_r = 3.2$, tan $\delta = 0.01$) (Abadia et al., 2009), and Silastic MDX−4210 Biomedical−Grade Base Elastomer ($\varepsilon_r = 3.3$, tan $\delta \approx 0$) (Karacolak et al., 2010).

Miniaturization Dimensions of the traditional half-wavelength (λ/2) or quarter-wavelength (λ/4) antennas at the frequency bands allocated for medical implants, and especially at the low-frequency MICS band, make them useless for implantable applications. Therefore, miniaturization becomes one of the greatest challenges in implantable antenna design.

Human tissue in which implantable antennas are intended to operate exhibits relatively high permittivity or, equivalently, reduced wave propagation velocity, which, in turn, work to advantageously miniaturize the physical size of the antenna. Use of patch designs for implantable antennas allows for several additional miniaturization techniques, including:

1. *Use of High−Permittivity Dielectric Materials* High-permittivity dielectrics are selected for implantable patch antennas [e.g. ceramic alumina ($\varepsilon_r = 9.4$) (Kiourti et al., 2011) or Rogers 3210 ($\varepsilon_r = 10.2$) (Kiourti and Nikita)] because they shorten the effective wavelength and result in lower resonance frequencies, thus assisting in antenna miniaturization.
2. *Lengthening of Current Flow Path on Patch Surface* Longer effective current flow paths excited on the radiating patch can bring the resonance frequency to lower values and achieve a more compact size for the implantable antenna. Meandered (Kiourti and Nikita, 2011), spiral (Kiourti and Nikita, 2011), waffle-type (Soontornpipit et al., 2005) and hook-slotted (Liu et al., 2008) shaped patches have been suggested for this purpose.
3. *Addition of Shorting Pins* Inserting a shorting pin between the ground and patch planes increases the effective size of the antenna, and, in turn, reduces the required physical dimensions, given a specific operation frequency scenario.

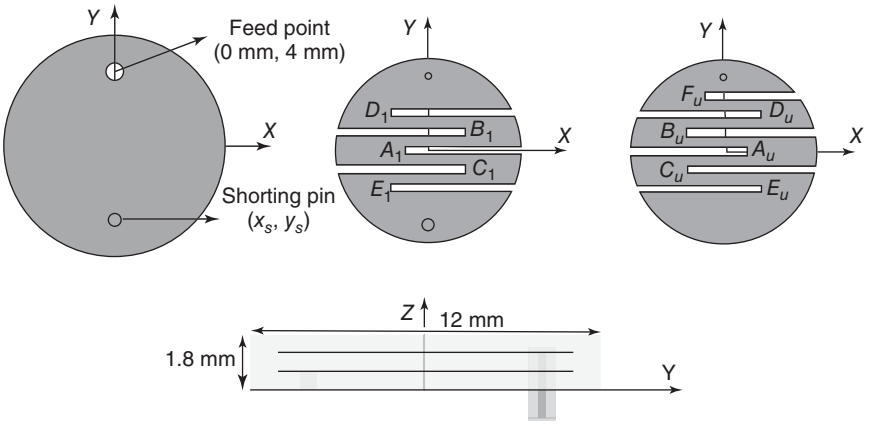

Figure 8.9 Example of a miniature skin-implantable MICS antenna (Kiourti and Nikita, 2012b).

The technique works in much the same way a ground plane doubles the height of a monopole antenna, that is, it typically produces a PIFA with the same resonance performance as a double-sized antenna without the shorting pin (Soontornpipit et al., 2004).

4. *Patch Stacking* Vertically stacking two radiating patches reduces antenna size by increasing (nearly doubling) the length of the current flow path (Kiourti and Nikita, 2012b).

   An example of a skin-implantable antenna that operates in the MICS band and employs all aforementioned techniques to reduce size is shown in Figure 8.9 (Kiourti and Nikita, 2012b). The model is parameterized to include variable-length meanders [denoted by the x coordinate (x_{ij}) of the points marked as $\{ij,\ i = A–F,\ j = \text{l},u\}$] and a variable positioned shorting pin (x_s, y_s), and the two-step design methodology of Figure 8.10 can be applied to optimize its resonance characteristics for any implantation scenario, in an accurate and fast way (Kiourti and Nikita, 2012b, 2012c). The methodology consists of an initial approximate design inside a tissue-simulating cube, and further quasi-Newton optimization inside a canonical model of the intended implantation site.

Patient Safety Considerations Patient safety issues limit the maximum allowable power incident to the implantable antenna. The specific absorption rate (SAR) (rate of energy deposited per unit mass of tissue) is generally accepted as the most appropriate dosimetric measure, and compliance with international guidelines is assessed. For example, the Institute of Electrical and Electronics Engineers (IEEE) C95.1–1999 standard restricts the SAR averaged over any 1 g of tissue in the shape of a cube to less than 1.6 W/kg (SAR 1 g, max $\leq$ 1.6 W/kg) (IEEE, 1999). The International Commission on Non-Ionizing Radiation Protection (ICNIRP) basic restrictions limit

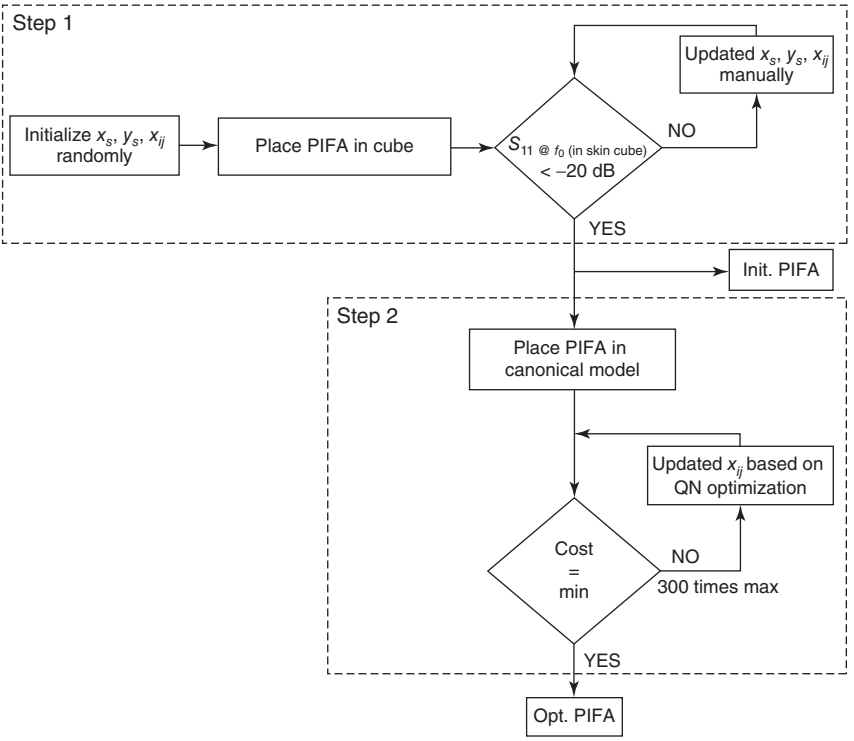

Figure 8.10 Proposed two-step methodology for implantable antenna design (Kiourti and Nikita, 2012b).

the SAR averaged over 10 g of contiguous tissue to less than 2 W/kg (ICNIRP, 1998). To harmonize with the ICNIRP guidelines, the IEEE C95.1–2005 standard restricts the SAR averaged over any 10 g of tissue in the shape of a cube to less than 2 W/kg (SAR 10 g, max $\leq$ 2 W/kg) (IEEE, 2005).

The power absorbed by the human body by an incident electromagnetic field is given by

$$P_{\text{abs}} = \frac{1}{2}\int \sigma |E|^2 dV \tag{8.3}$$

where σ is the conductivity of the human tissues, and $|E|$ is the intensity of the electric field inside the body. Absorbed power is, thus, related to the electric field, so that maximum SAR values are recorded in the areas where maximum electric field intensities occur.

Based on the deduction that peak averaged SAR values are generated from the high near field, advanced implantable patch antennas can be designed aiming at lower electric field intensities. An attempt to understand the radiation mechanism of an implantable antenna toward appropriately modifying its design for reducing the spatial-averaged SAR in human tissue has been presented in Kim and Rahmat-Samii (2006). Replacing the uniform-width spiral radiator of an implantable MICS PIFA

with a non-uniform-width radiator was found to decrease the electric field intensity and, in turn, SAR.

It is worth noting that, contrary to wearable antennas, the high local SAR values achieved for implantable antennas need to be considered more carefully due to higher local energy deposition from the RF source. High values of the local electric field induced in human tissues might even cause some nonthermal effects.

Multi-band Operation If operated continuously, the transceiver of the implantable medical device will consume significant energy and reduce the lifetime of the device. Even though methods for recharging the battery are available (e.g., via an inductive loop approach (Valdastri et al., 2004)), it would be highly advantageous to use the biotelemetry link only when necessary. For this purpose, a transceiver with dual-band operation may be used. The system uses two frequency bands, one for "wake-up," and one for transmission. The transceiver stays in "sleep mode" with a low power consumption until a wake–up signal is sensed in the 2.45 GHz ISM band. In the normal mode, the implantable medical device (IMD) is fully powered and exchanges data in the MICS band. Following the data transfer, the IMD transceiver returns back to the sleep mode.

For example, a dual-band (MICS and ISM) implantable antenna has been proposed in the literature for continuous glucose monitoring (Karacolak et al., 2008). A meandered antenna configuration was considered for optimizing the antenna surface area, and particle swarm optimization was applied to achieve the desired resonance characteristics (Figure 8.11*a*). An advanced antenna design was suggested using a π–shaped

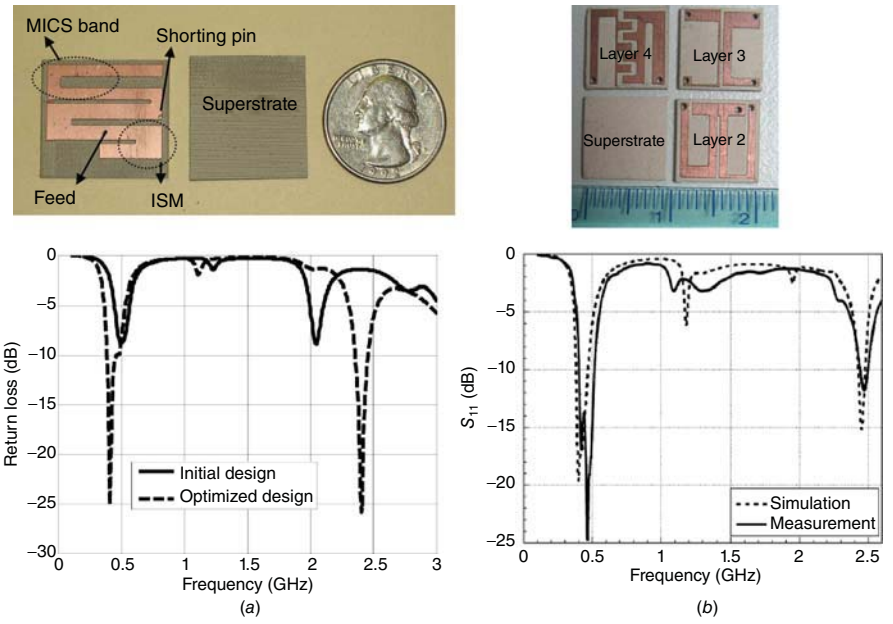

Figure 8.11 Geometry and reflection coefficient frequency response of (*a*) dual-band (Karacolak et al., 2008) and (*b*) triple-band (Huang et al., 2011) implantable antennas.

radiator with stacked and spiral structure, to support triple-band operation with data telemetry (402 MHz), wireless power transmission (433 MHz), and wake-up controller (2450 MHz) (Huang et al., 2011) (Figure 8.11*b*).

Influence of Human Body Several strategies have been proposed for implantable antenna design, which are mainly dictated by the fact that antennas are intended to operate inside biological tissue rather than in free space. The antenna should, therefore, be designed inside free space and further refined for tissue implantation or designed directly inside an environment surrounded by human tissue.

Rucker et al. (2007) designed a patch antenna operating in the MICS band in free space and further implanted it inside the skin tissue of an anatomical head model. A resonance frequency detuning was observed as attributed to the capacitive loading effect of the surrounding tissues, and a varactor diode with tuning capability was inserted to refine resonance.

In Abadia et al. (2009), a MICS antenna was designed in free space aiming at a high gain value (higher than − 20 dB) to account for subsequent body absorption losses. The antenna was optimized in free space to minimize size and further be covered by a biocompatible layer and placed inside tissue material. Design modifications were performed to account for the frequency shift induced by the presence of encapsulation and human tissue.

When designing implantable antennas directly inside tissue material, the simplest and fastest option is to use a single-layer tissue model of the intended implantation tissue. Following this methodology, antennas are designed for a "generic" tissue implantation scenario. Simplified tissue models in the shape of a cube (Kiourti and Nikita, 2011, 2012b, 2012d; Kiourti et al., 2011; 2013), a rectangular parallelepiped (Liu et al., 2008), and a cylinder (Liu et al., 2009) have been used for this purpose. Design is performed by selecting the dielectric material, and subsequently optimizing all antenna design parameters to refine tuning at the desired operation frequency. Another option is to design the antenna for a specific implantation site. A multilayer tissue model is selected in this case, with either finite or infinite dimensions. For example, implantable antennas intended for trunk (Karacolak et al., 2008) and chest (Kim and Rahmat-Samii, 2004) implantation have been directly designed inside three-layer planar tissue models consisting of skin, fat, and muscle tissues.

An advanced two-step design methodology was proposed for implantable antennas that emphasizes design speed-up and optimized resonance performance inside specific implantation sites (Kiourti and Nikita, 2012b). This involves approximate antenna design inside a simplified tissue model (a cube filled with the intended tissue material) and further quasi-Newton optimization inside a canonical model of the intended implantation site. Despite being optimized inside a canonical tissue model, the designed antennas were shown to exhibit insignificant resonance discrepancies inside detailed anatomical tissue models (Kiourti and Nikita, 2013).

Experimental Investigations Prototype fabrication of implantable antennas meets all classical difficulties of miniature antennas. For example, additional glue layers used to affix all components together strongly affect antenna performance by shifting

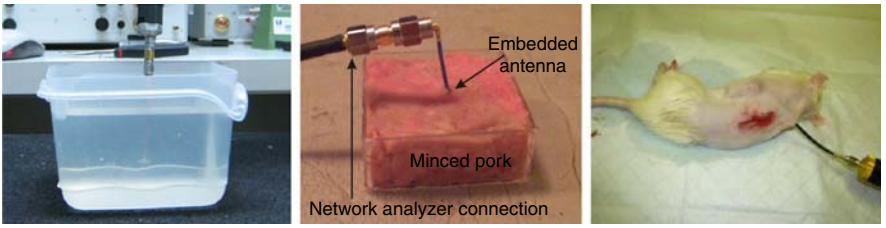

Figure 8.12 Experimental investigations for implantable antennas: (*a*) in vitro testing (Kiourti and Nikita, 2012b), (*b*) testing inside animal tissue samples (Huang et al., 2011), and (*c*) in vivo testing (Karacolak et al., 2010). (*See insert for color representation of b and c*.)

its resonance frequency and degrading its matching characteristics. Furthermore, the coaxial cable feed used to connect the antenna with the network analyzer may give rise to radiating currents on the outer part of the cable, thus deteriorating measurements. Based on the above, design parameters of the numerical antenna model must be slightly adjusted to take prototype fabrication considerations into account.

Testing inside phantoms is relatively easy and practical to implement. The fabricated prototype is immersed inside a tissue phantom (i.e., a container filled with a liquid or gel material that mimics the electrical properties of biological tissue) and measured (Figure 8.12*a*). Reflection coefficient measurements are performed by immersing the prototype antenna inside a tissue-emulating phantom and connecting it to a network analyzer through a coaxial cable.

Use of animal tissue samples provides an easy approach to mimicking the frequency dependency characteristic of the electrical properties of tissues (Figure 8.12*b*). This can prove highly advantageous when carrying out measurements for multiband implantable antennas. In the literature, an implantable dual-band patch antenna that resonates at 380 and 440 MHz has been tested inside test tissue obtained by grinding the front leg of a pig (Lee et al., 2009). A dual-band skin-implantable patch antenna operating in the MICS and 2450 MHz ISM bands has also been tested in real animal skin (Karacolak et al., 2009). Skin samples were extracted from the dorsal area of three donor rats to cover the designed antenna, and measurements were performed within 30 min of euthanization. Finally, a triple-band implantable patch antenna has been tested inside a minced front leg of a pig (Huang et al., 2011).

In vivo testing inside living animals is highly challenging too (Figure 8.12*c*). An in vivo testing protocol needs to be developed before the experimental investigations, which will deal with the choice and number of animals, presurgical preparation, anesthesia, surgical procedure, measurements, and postsurgical treatment. In vivo studies reported in the literature are very limited. The return loss frequency response of a skin-implantable antenna has been measured using rats as model animals (Karacolak et al., 2010). The antenna was implanted by means of a surgical operation inside the dorsal midline of three rats, and euthanasia was applied after the measurements (approximately 13–15 min after the surgery). Canine studies for trans-scalp evaluation of a scalp-implantable antenna at 2450 MHz have also been

presented (Kawoos et al., 2008). Canine models were selected to ensure a large head size, and an intracranial pressure monitoring device with an integrated PIFA was fixed to the skull. The monitor was tested while the dog was still under anesthesia. After the measurements, the animal was allowed to emerge from anesthesia and taken to the recovery area.

8.4.2 Channel Modeling

Modeling the biomedical telemetry channel for implantable antennas is a highly challenging task. Unlike free-space propagation, the various tissues and organs within the body have their own unique electrical characteristics, the lossy medium absorbs electromagnetic (EM) energy, and the presence of objects causes EM field refraction, diffraction, reflection, and absorption.

Transmission Coefficient Studies Even though most studies for implantable antennas are limited to reflection coefficient, radiation pattern, and safety investigations, transmission coefficient (S_{21}) and numerical and experimental results have also been presented:

- Warty et al., (2008) implanted 2.45 GHz PIFA inside a gel scalp phantom for intracranial pressure monitoring, and a linearly polarized 2.45 GHz chip antenna was used as the receiving (probing) antenna. Transmission coefficient measurements were reported for the first time. The drift of the transmission coefficient values over time was evaluated, and the effective radiated power (ERP) was computed from the transmission measurements. An increase in S_{21} of 2.2−2.4 dB was observed over a period of two days. Transmission measurements performed using both S_{21} and the received power measurement (for an intracranial pressure device mimic) yielded a maximum ERP of approximately 2 mW per 1 W of power delivered to the antenna. Values of the received power (P_r) and ERP per 1 W delivered to the PIFA are shown in Figure 8.13*a* as a function of distance.
- Weiss et al. (2009) presented simulations and measurements for a 433 MHz mock telemetry link in a 6 cm-thick porcine thigh. Electrically, short linear wire antennas were used at both the embedded transmitter and external receiver, whereas the receiver was considered to be placed on the outer surface of the thigh. Simulated and measured S_{21} values in the porcine experiments are shown in Figure 8.13*b* and are found to vary in the −45 to −55 dB range for different transmitter-to-receiver distances. Simulations for a 10 cm-radius cylindrical human thigh and a 3 cm-long receiver antenna demonstrated a coupling coefficient of −63 dB. When a 6 cm-long external antenna was used as the receiver, S_{21} increased to −54 dB, a 9 dB improvement. The lowest coupling was computed for muscular patients. To accommodate such a patient with a thigh radius of 21 cm, a 30 dB link margin was found to be required as compared to the average male.

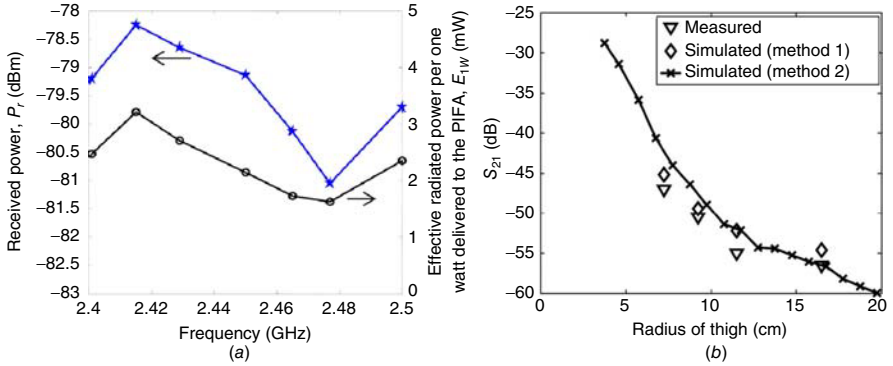

Figure 8.13 (*a*) Values of the received power (P_r) and ERP per 1 W delivered to the PIFA as a function of distance from a receiving chip antenna (Warty et al., 2008) and (*b*) simulated and measured S_{21} values in the porcine experiments of Weiss et al. (2009).

Out-of-Body Channel Modeling Link budget investigations have also been carried out for implantable antennas. Characteristic studies are summarized below.

- A link budget calculation was proposed for the communication between a left-ventricular wireless implant and an off-body base station, as an example for MICS applications (Sani et al., 2009). In far-field communication in free space, the received power at the base station was calculated using the Friis formula:

$$P_r = P_t(1 - |S_{11}|^2)G_t\left(\frac{\lambda}{4\pi d}\right)^2 G_r(1 - |S_{22}|^2) \tag{8.4}$$

where $|S_{11}|$ and $|S_{22}|$ are the reflection coefficients of the transmitting and the receiving antennas, P_t is the transmitter's available power, G_t is the gain of the implantable transmitting antenna, G_r is the gain of the exterior receiving antenna, λ is the free-space wavelength, and d is the distance between the transmitter and the receiver.

In the indoor environment, due to reflections, diffraction, and scattering of electromagnetic waves, the transmitted signal reaches the receiver via more than one path. The most common path loss (PL) model, that is, the log-distance model, was suggested, so that

$$\text{PL}(d)\ (\text{dB}) = 10 \cdot n \log\left(\frac{d}{d_0}\right) + \text{PL}(d_0) \tag{8.5}$$

where n indicates how fast the received power decays with distance, d_0 is a reference distance, chosen to be 1 m, and $\text{PL}(d_0)$ is the PL value at the distance d_0, which is assumed to be equal to the free-space loss.

The received power at the exterior base station is then calculated as

$$P_r\ (\text{dBm}) = P_t\ (\text{dBm}) + G_t(\text{dB}) - \text{PL}(\text{dB}) + G_r\ (\text{dB}) \tag{8.6}$$

Furthermore, it was demonstrated, that due to the presence of human tissues, the antenna radiation from wireless implants tended to be directive, and, therefore, the SNR in the communication link was strongly dependent on the orientation of the human subject with respect to the base station.

- The wave propagation between an off-body reader and an ultra-high-frequency (UHF) (868 MHz) subcutaneous tag antenna has also been investigated (Sani et al., 2010). Both LOS and NLOS scenarios were studied, and Equations (8.2)–(8.4) were applied.

  Results demonstrated that, due to the body losses, the electrically small size of the antenna, and the directional radiation pattern, a passive tag solution allows a very limited communication range. If the tag is powered (active tag) with a limited power (−20 dBm), a maximum communication range of 10 m was calculated for propagation within a room.

- Propagation losses of body-implanted antennas have been studied at the ISM bands of 433, 915, 2450, and 5800 MHz (Gemio, 2010). A single- and a three-layer body models were used, and the antenna pair gain was analyzed at different depths of the implantable antenna. Free-space wireless links were assumed between half-wavelength resonant dipole antennas, and Equation (8.4) was applied to investigate the link budget.

  Simulation results proved that, when far-field conditions are fulfilled, body losses can be included in the gain of the implanted antenna, and a free-space propagation model can be assumed to evaluate the system link budget. The single-layer model was found to be a conservative approach that tended to underestimate the antenna pair gain as compared to the three-layer model. Changes in frequency revealed a trade-off between antenna dimensions and system performance. When the frequency was doubled, antenna dimensions were reduced by half, and propagation losses were increased by 6 dB, whereas the antenna pair gain was further degraded due to the higher loss of body tissues. Similar trade-offs were observed when the antenna position was changed from one layer to another.

- Finally, Xia et al. (2009) carried out a link budget calculation between a 2.45 GHz H-shaped cavity slot antenna implanted in a human arm and a receiving monopole antenna placed 4 m away inside a sickroom. The availability of communication was decided by the C/N_0 ratio, that is, if the link's C/N_0 exceeds the required C/N_0, then wireless communication is possible. Table 8.3 shows the parameters used to calculate the link C/N_0 and the required C/N_0. The link C/N_0 and the required C/N_0 used were calculated as follows.

$$\text{Link } \frac{C}{N_0} = P_t - L_{\text{feed}} + G_t - L_f - L_a + G_r - L_{\text{feed}} - N_0 \qquad (\text{dB/Hz}) \tag{8.7}$$

$$\text{Required } \frac{C}{N_0} = \frac{E_b}{N_0} + 10\log_{10}(B_r) - G_c + G_d \qquad (\text{dB/Hz}) \tag{8.8}$$

TABLE 8.3 Parameters Used to Calculate Link and Required Signal-to-Noise Ratio

Transmitter		Propagation	
Frequency f (GHz)	2.45	Distance d (m)	4
Transmitter power P_t (W)	1.25×10^7	Free-space loss L_f (dB)	52.27
Feeding loss L_{feed} (dB)	1.0	Air propagation loss L_a (dB)	0.5
Transmitter antenna gain G_t (dBi)	− 26.5		
Receiver		**Signal Quality**	
Receiver antenna gain G_r (dBi)	2.15	Bit rate B_r (kbps)	7
Feeding loss L_{feed} (dB)	1	Bit error rate	1×10^{-5}
Ambient temperature T_0 (K)	293	E_b/N_0 (ideal PSK) (dB)	9.6
Receiver noise factor NF (dB)	3.5	Coding gain G_c (dB)	0
Boltzmann constant k	1.38×10^{-23}	Fixing deterioration G_d (dB)	2.5
Noise power density N_0 (dB/Hz)	− 199.95		

Source: Xia et al. (2009).

$$L_f = 10 \log_{10}\left(\frac{4\pi d}{\lambda}\right)^2 \quad \text{(dB)} \tag{8.9}$$

$$N_0 = 10 \log_{10}(k) + 10 \log_{10}(T_i) \quad \text{(dB/Hz)} \tag{8.10}$$

$$T_i = T_0(\text{NF} - 1) \text{ (K)} \tag{8.11}$$

In the scenario under study, the link was computed to be higher than that required by approximately 0.3 dB.

Inside-the-Body Channel Modeling In estimating the propagation loss for wireless transmission inside the human body, changing the loss coefficient of the free-space formula will only change the rate of decrease in power and will not help in estimating the total loss in the form of absorption.

A propagation loss model for homogeneous tissue bodies (PMBA) was reported in Gupta et al. (2003) and verified for the frequency range 900 MHz to 3 GHz, both numerically and experimentally. The study considered an elemental oscillating electric dipole in a lossy medium of conductivity σ, permittivity ε, permeability μ, complex propagation constant γ, complex intrinsic impedance $\eta = \gamma/(\sigma + j\omega\varepsilon)$ at frequency ω, as shown in Figure 8.14*a*. The dipole consisted of a short conducting wire of length *dl*, terminated in two small conductive spheres or disks, whereas the current *I* was assumed to be uniform and vary sinusoidally with time. The power absorbed in the near field of the lossy tissue was said to be obtained by computing the average SAR over the entire tissue mass in the near field, that is, from the surface of the antenna ($R = r$) to the end of the near-field region ($R = d_0$, where d_0 is the point where the far field starts), as

$$P_{\text{NF}} = \sigma\mu\omega \frac{|\eta|}{|\gamma|} \frac{I^2 dl^2}{6\pi}(A + B + C) \tag{8.12}$$

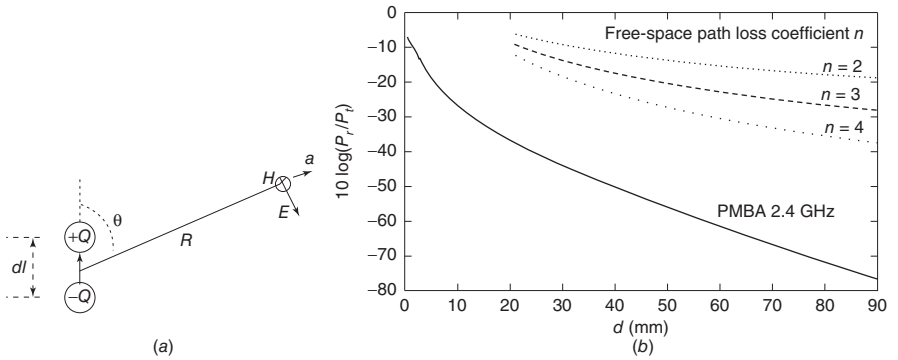

Figure 8.14 Development of propagation model for in-body transmission: (*a*) a Hertzian dipole and (*b*) comparison of the proposed model with the free-space loss formula (Gupta et al., 2003).

where

$$A = e^{-2\alpha r}\left[\frac{|\gamma|^2}{2\alpha} + \frac{d_0 - r}{4r^2} + \frac{|\gamma|(d_0 - r)}{2r}\right] \tag{8.13}$$

$$B = e^{-2\alpha d_0}\left[\frac{-|\gamma|^2}{2\alpha} + \frac{d_0 - r}{4d_0^2} + \frac{|\gamma|(d_0 - r)}{2d_0}\right] \tag{8.14}$$

$$C = e^{-\alpha(d_0 + r)}\left[\frac{2\left(d_0 - r\right)}{(d_0 + r)^2} + \frac{2|\gamma|(d_0 - r)}{(d_0 + r)}\right] \tag{8.15}$$

The total power absorbed in the far field of the lossy tissue between the transmitting and receiving antennas was said to be obtained by computing the average SAR over the entire tissue mass in the far field from distance d_0 to d as

$$P_{\text{FF}} = \sigma|\eta|^2|\gamma|^2\frac{I^2 dl^2}{12\pi\alpha}(e^{-2\alpha d_0} - e^{-2ad}) \tag{8.16}$$

The ERP is obtained by subtracting the loss in the near field (P_{NF}) and the far field (P_{FF}) from the transmitted power P_t (i.e., $(P_t - P_{\text{loss}})G_t$), where

$$P_{\text{loss}} = P_{\text{NF}} + P_{\text{FF}} \tag{8.17}$$

The power received by the receiving antenna in the near field was approximated by

$$P_r = \frac{16\delta(P_t - P_{\text{NF}})}{\pi L^2}A_e \tag{8.18}$$

where L is the largest dimension of the antenna, and δ is the aperture efficiency (approximated as $\delta = A_e/A$, with A_e being the effective aperture, and A the physical area of the antenna).

The power received by the receiving antenna in the far field was calculated as

$$P_r = \frac{(P_t - P_{\mathrm{NF}} - P_{\mathrm{FF}})\lambda^2}{(4\pi d)^2} G_t G_r \tag{8.19}$$

where G_t and G_r are the gains of the transmitting and receiving antennas.

Figure 8.14*b* compares PMBA with the free-space propagation model $P_r = P_t G_t G_r \left[\lambda/4\pi \mathrm{d}\right]^{\mathrm{n}}$ with loss coefficients $n = 2, 3, 4$. It is observed that power received in PMBA decreases more rapidly than free-space loss. Compared to free space, there is an additional 30–35 dB of attenuation at small distances in the far field.

It is worth noting that even though the derived formulas are applicable only in the case of small dipole implantable antennas, the power loss formula for similar applications with other antennas could be derived in a similar manner.

8.5 INGESTIBLE ANTENNAS

The conventional methods used for diagnosing disorders of the human gastrointestinal (GI) tract cause significant patient discomfort. As a result, there is considerable ongoing work in developing ingestible antennas that can be integrated into a capsule and swallowed for examination of the entire digestive tract.

8.5.1 Antenna Design

Selection of Operation Frequency Selection of operation frequency for ingestible antennas has received significant attention from the scientific community. The reason is that selection of frequency is accompanied by a number of competing effects. For example, antenna efficiency can improve with frequency. On the other hand, higher frequencies may cause increased radiation absorption because of the high water content of body tissues. This in turn may deteriorate the performance of the wireless link, requiring increased levels of supply powers and posing questions regarding patient safety.

The effects of the human body on the performance of an ingestible antenna inside the frequency range of 150 MHz–1.2 GHz have been investigated in Chirwa et al. (2003a). Maximum radiation was found to occur between 450 and 900 MHz, whereas radiation intensity outside the body had a Gaussian form relationship with frequency. Although the frequency range under study covered the ISM bands of 434 and 915 MHz, these bands are not well developed for digital video transmission. Chirwa et al. (2003b) found a peak in the power transmitted by an ingestible medical device at approximately 650 MHz, and adequate communication performance was demonstrated between 600 MHz and 1 GHz.

On the other hand, video transmission in the 2.45 GHz band is better developed for WLAN and Bluetooth applications in terms of technology, antennas, camera modules, and other RF components. Furthermore, ingestible medical devices operating at this frequency can be directly connected to the WLAN or Bluetooth networks for real-time monitoring and remote control. Finally, higher transmission frequencies allow the use of smaller antennas and electronic components, which is a prerequisite for ingestible medical devices. Therefore, the 2.45 GHz band appears to be a promising solution. For example, an IC design for wireless capsule endoscopy at 2.4 GHz has been proposed in Xie et al. (2004).

By taking into account that the whole ingestible telemetry system has about 80–110 dB of room for loss in system efficiency and body tissue attenuation, it becomes obvious that ingestible medical devices operating at 5.8 GHz can also be applied. Attenuation achieved by such devices is expected to be within the desired attenuation range; however, great care must be taken to design an efficient telemetry system without (or minimum) additional losses.

Type and Material of Antenna Different from implantable antennas, the ingestible antenna needs to be omnidirectional and exhibit circular polarization in order to transmit signals independent of its position and orientation. Since the capsule device travels along the entire GI tract, its exact position and orientation are generally unknown. Therefore, an isotropic radiation pattern is required for ingestible antennas.

Given the above considerations, normal mode helical antennas are most commonly employed for such applications (Figure 8.15*a*). Furthermore, as wireless capsule endoscope systems transmit real-time and high-resolution data, antennas with a miniature size but wide bandwidth are required. For example, a wideband spiral antenna for ingestible capsule endoscope systems at 500 MHz was presented (Lee et al., 2011) (Figure 8.15*b*). A thick-arm spiral structure was applied to achieve a fractional bandwidth of 21% and an isotropic radiation pattern.

Numerical modeling of ingestible antennas is also intriguing. For example, although the FDTD method is able to model anatomically detailed human body

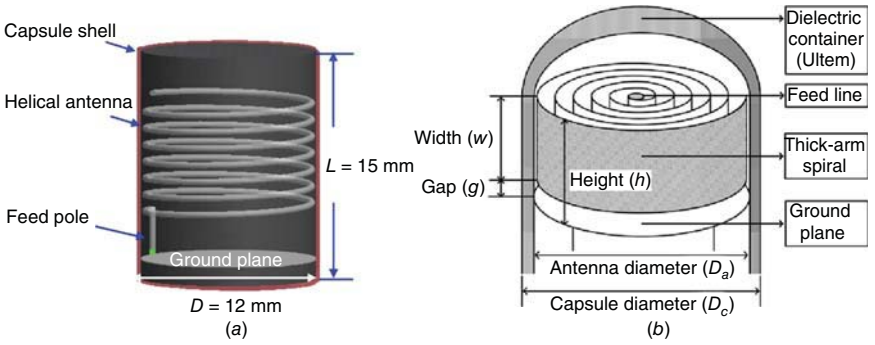

Figure 8.15 Example ingestible antennas: (*a*) helical (Xu et al., 2009b), and (*b*) spiral (Lee et al., 2011) geometries.

structures, there are still significant difficulties in modeling small antennas. Furthermore, it is important to highlight that employing a one-cell (delta gap) excitation in FDTD simulations, where the excitation feed gap corresponds to one entire spatial interval of the FDTD lattice, is not effective. In such cases, the size of the feeding gap is expected to be comparable with that of the antenna to be modeled, thus resulting in erroneous numerical results.

Same as for implantable antennas, ingestible antennas must be biocompatible so that they do not harm the patient and durable so that the body fluids do not harm the antenna. These requirements entail packaging of the ingestible antennas inside a shell. Capsule casings and circuitry have been found to have a negligible effect on the performance of the ingestible antenna. Therefore, taking the effects of casing into account while modeling the antenna is not necessarily compulsory.

Patient Safety Considerations Safety performance of ingestible antennas operating at several frequency bands attracts significant scientific interest. Usually, low-frequency wireless devices cause less significant biological effects than higher-frequency devices as attributed to decreased levels of tissue absorption. Design of an ingestible antenna at high frequencies needs to be carefully considered in order to guarantee compliance with safety guidelines.

The SAR and temperature rise performance of ingestible antennas has been analyzed at frequencies from 430 MHz to 3 GHz (Xu et al., 2008b). Simulations were carried out inside a high-fidelity human body model consisting of 34 types of tissues, and a helical ingestible antenna was considered inside a plastic capsule with a diameter and length of 12 and 5 mm, respectively. Results showed that high values of SAR and temperature rise were localized at the area near the location of the ingestible device. Figure 8.16 shows the near-field intensities both inside and outside the human body model at frequencies of 430 MHz, 800 MHz, 1.2 GHz, 2.4 GHz, and 3 GHz. The ingestible antenna was safe and could be used in ingestible medical devices at input power levels of less than 25 mW in order to conform with safety regulations.

Simulation results for a helical ingestible antenna at 2.4 GHz, carried out in 21 scenarios (3 orientations at 7 source positions), showed that all temperature rises, peaks of the SAR, and averaged SAR values were under the safety limits when the delivered power was no more than 26.16 mW (Xu et al., 2008a). In other words, the frequency of 2.4 GHz was proved to be able to be employed safely and efficiently in the ingestible wireless device, as long as its input power is no more than 26.16 mW.

Xu et al. (2009b) assessed the compliance of ingestible medical devices with international safety guidelines at 430, 800, 1200, and 2400 MHz. A high-fidelity female body with 34 types of tissues and a high-fidelity male body with 23 types of tissue, and scaled into the same height with the female body, were studied. Among all simulated scenarios, the maxima of the 1 g and 10 g averaged SAR were computed as 3.71 and 1.37 W/kg at an input power of 25 mW, respectively. The ingestible antenna was found to be safe to be applied in the medical device at an input power less than 36 and 11 mW according to the ICNIRP and IEEE safety standards, respectively. As far

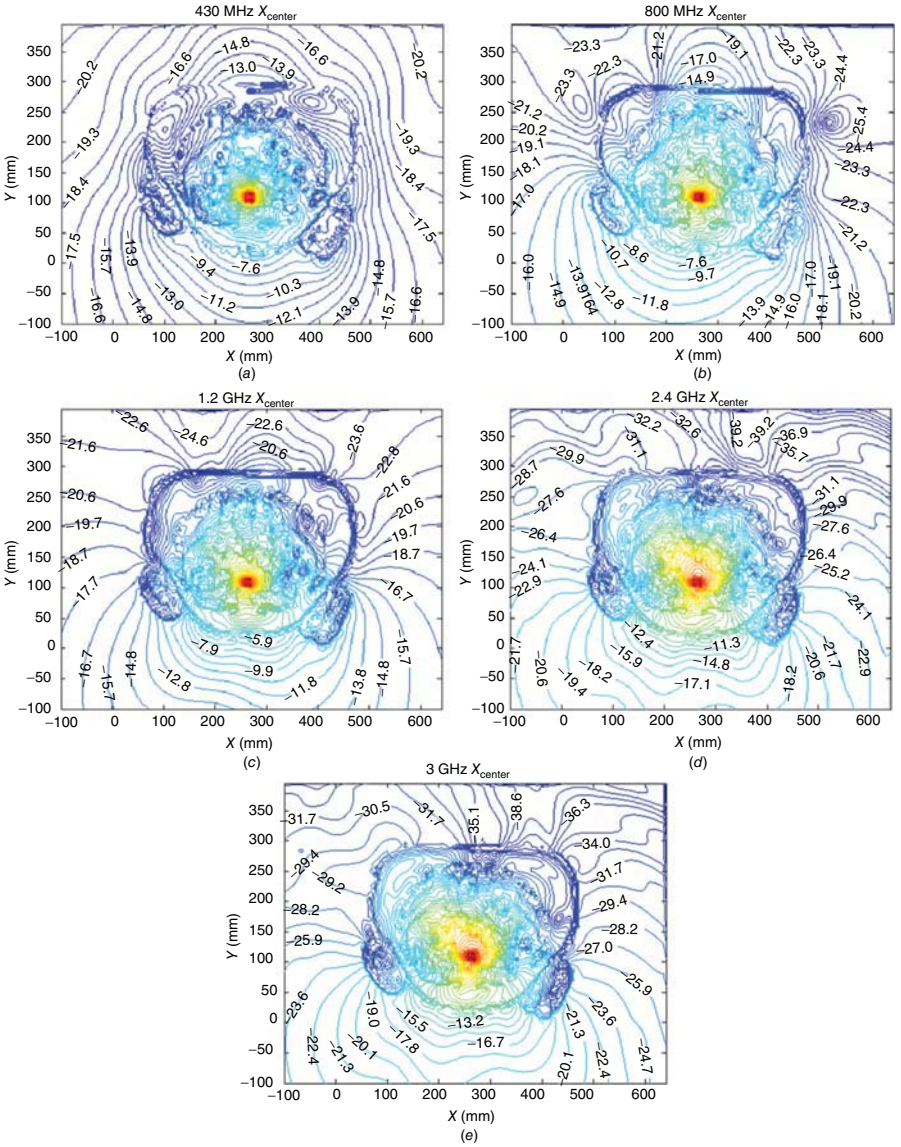

Figure 8.16 Near fields for ingestible antenna at (*a*) 430 MHz, (*b*) 800 MHz, (*c*) 1.2 GHz, (*d*) 2.4 GHz, and (*e*) 3 GHz (Xu et al., 2008b). (*See insert for color representation of the figure.*)

as the thermal effect is concerned, it was shown that even in the cases of maximum SAR values, temperature rise maxima remained low.

Finally, in Xu et al. (2009a), the safety performance of ingestible antennas was evaluated in two (male, female) realistic human body models whose dielectric parameters (permittivity and conductivity) were varied from the original by ±10% and ±20%. Three operation frequencies were considered, that is, 430, 800, and 1200 MHz. SAR values were found to increase with the increase in conductivities of human body tissues, and usually decreased with the increase in permittivities. From the equation of SAR calculation, one might have assumed that the SAR value would increase with the increment of dielectric values. However, SAR values are not only influenced by the dielectric properties of the medium but also by impedance matching, which is, in turn, influenced by the dielectric properties. A variation by up to 20% in conductivities and permittivities alone or simultaneously always caused a SAR variation by less than 10, 20, and 30% at 430, 800, and 1200 MHz, respectively. The ingestible antenna was shown to be safe used at input power levels less than 12.6, 9.3, and 8.4 mW, according to the IEEE safety standards at 430, 800, and 1200 MHz, respectively. SAR depositions in the female body model were larger than those in the male body model.

Position and Orientation Considerations Performance of ingestible antennas for various locations inside the body and antenna orientations has also been investigated.

Chirwa et al. (2003a) performed FDTD numerical investigations considering a male human subject and an ingestible monofilar helix antenna with a diameter of 8 mm, length of 4 mm, and pitch of 1 mm (four turns). Frequencies were in the range 150 MHz–1.2 GHz. Three antenna orientations were investigated (vertical, transverse, and longitudinal), and simulations were performed at many locations inside the GI tract, as shown in Figure 8.17*a*. Near- and far-field results showed that maximum radiation was experienced on the anterior side of the body, while no direct correlation was found between the near and far fields. For the majority of locations, vertically polarized radiation was more greatly attenuated than horizontal radiation. Anatomy around the gut region highly affected the electromagnetic field results, while radiation characteristics differed significantly based on the distance between the ingestible antenna and the outer surface of the body.

In another study, the same monofilar helix antenna was used, and simulations were carried out for five locations in the GI: near the skin, top of the small intestine, behind the stomach, right extremity of the small intestine next to the colon, a central location, and the bottom of the small intestine (Chirwa et al., 2003b). Results showed that the exact location of the ingestible antenna had a strong effect on radiation. The radiated field was predominantly strongest in the same horizontal transverse plane as the source and in the direction that was on the line from the source to the nearest body surface. Therefore, the optimum location for a receiver antenna would be an anterior location slightly to the left of the abdomen (as the small intestine does not extend so much to the right due to the presence of the colon).

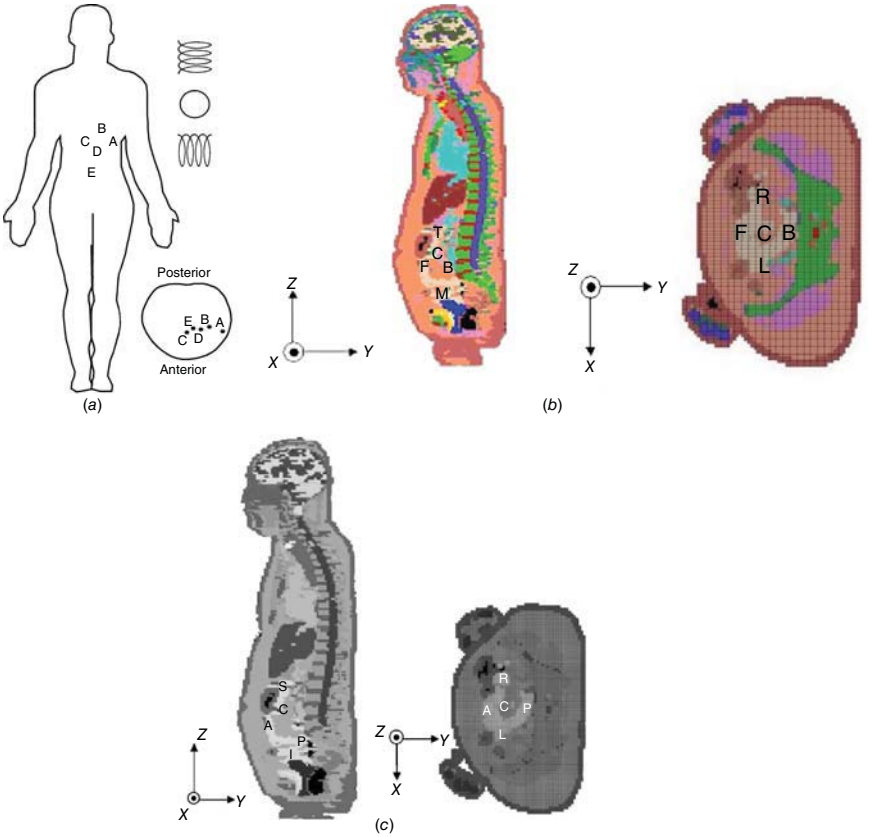

Figure 8.17 Location and orientation of ingestible antennas in (*a*) Chirwa et al. (2003a), (*b*) Xu et al. (2008a, 2008b), and (*c*) (Xu et al., 2009b).

Numerical analyses have further been carried out for three orientations of an ingestible antenna at frequencies from 430 MHz to 3 GHz, and at seven positions inside a human body model (Figure 8.17*b*) (Xu et al., 2008*b*). A helical antenna was assumed that was integrated inside a plastic shell with a thickness of 1 mm, a diameter of 12 mm, and a length of 15 mm. It was shown that the orientation and position of the ingestible antenna, which gave maximum radiation efficiency, was frequency dependent. Furthermore, when the ingestible antenna was located at the frontmost and backmost positions of the small intestine, the electric intensity outside the human body was maximum and minimum, respectively. Position was found to influence the radiation efficiency of the antenna more than its orientation.

Simulations carried out for a 2.4-GHz ingested source at 3 orientations and 7 positions (Figure 8.17*b*) demonstrated that port impedances, radiation efficiencies, and link performance for the antenna varied greatly with location and orientation

(Xu et al., 2008a). Similarly, Xu et al. (2009b), assessed ingestible antennas for 21 scenarios (3 orientations, 7 positions) at 430, 800, 1200, and 2400 MHz (Figure 8.17*c*). Radiation characteristics and radiation absorption were found to be frequency, position, and orientation dependent. The study demonstrated that if the motion of the ingestible antenna inside the GI tract could be controlled, then the quality of communication would be improved by 3 dB at least. The electric field intensity in the anterior of the human body was higher than that in the posterior.

8.5.2 Channel Modeling

Only a limited number of research studies have been performed regarding the modeling of the channel between an ingestible antenna integrated into an ingestible medical device and an exterior antenna integrated into an exterior monitoring/control device. For example, an attempt has been made to estimate the attenuation of the human body trunk for ingestible antennas in the frequency range of 100 MHz–6 GHz (Chan et al., 2005). A simplified rectangular ($55 \times 24 \times 16$ cm^3) phantom was used to emulate the human trunk, which was filled with distilled water, saline solution, and porcine tissue alternately (Figure 8.18*a*). Patch antennas matched at 300 MHz, 900 MHz, 1.5 GHz, 3.0 GHz, and 4.8 GHz were used as radiating sources inside the model, whereas a broadband yagi antenna and a broadband horn antenna were used as the receiving antennas for the frequency ranges of 100 MHz–1.3 GHz and 1.5 GHz–6 GHz, respectively. The received power considering free space, the tank filled with distilled water, the tank filled with saline solution, and the tank filled with porcine tissue were denoted as $P_{r,\text{air}}$, $P_{r,\text{water}}$, $P_{r,\text{saline}}$, and $P_{r,\text{tissue}}$, respectively. With these values recorded, attenuation of different water and saline solutions was calculated as

$$\text{Attenuation in water (dB)} = P_{r,\text{air}}\ (\text{dBm}) - P_{r,\text{water}}\ (\text{dBm}) \tag{8.20}$$

$$\text{Attenuation in saline (dB)} = P_{r,\text{air}}\ (\text{dBm}) - P_{r,\text{saline}}\ (\text{dBm}) \tag{8.21}$$

$$\text{Attenuation in porcine tissue (dB)} = P_{r,\text{air}}\ (\text{dBm}) - P_{r,\text{tissue}}\ (\text{dBm}) \tag{8.22}$$

Averaged attenuation values were plotted as shown in Figure 8.18*b*. For comparison purposes, an ideal curve of the attenuation exhibited for a plane wave traveling through 6 cm of water (Debye equations) is also plotted. All curves indicated a similar trend of attenuation. Since the ideal curve considered the attenuation of water in only one dimension, experimental data appear as reasonable and reliable. Saline solution exhibited higher attenuation than water (by 5–15 dB), as attributed to its higher conductivity. Attenuation within porcine tissue laid between the water and saline curves.

Link budget studies have also been performed. Rajagopalan and Sahmat-Samii (2010) developed a link budget for ingestible antennas based on frequency, SAR, and

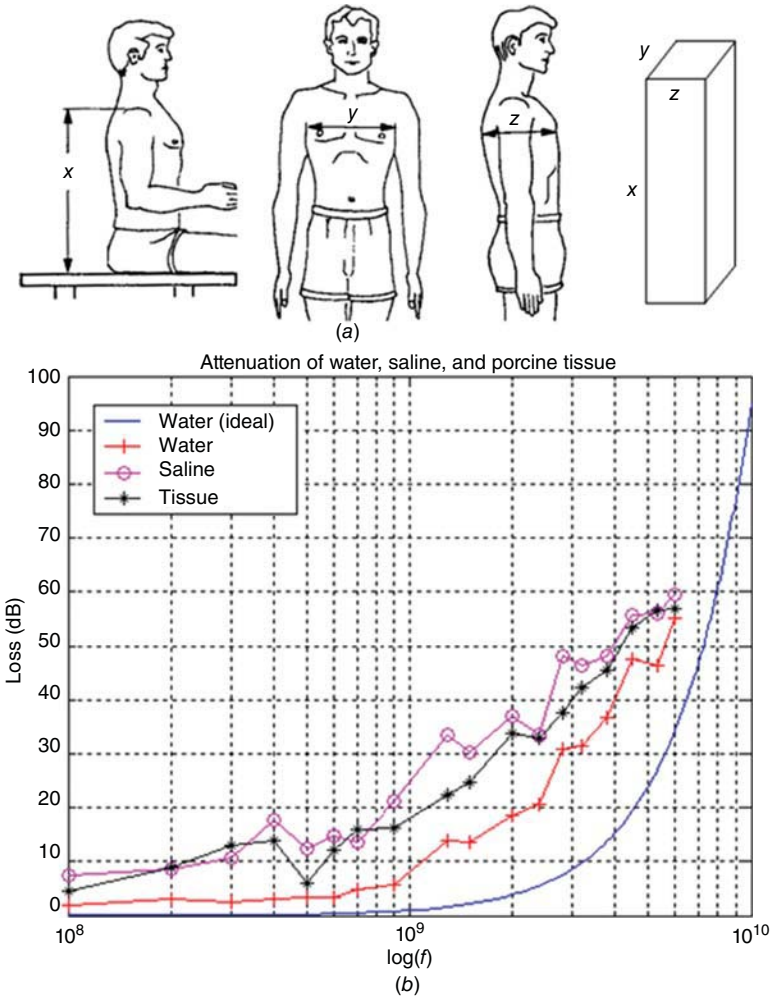

Figure 8.18 Estimation of attenuation of the human body trunk for ingestible antennas: (*a*) simplified phantom of the human body trunk and (*b*) attenuation of water, saline solution, and porcine tissue (Chan et al., 2005).

power limitations, and it was applied to assess the performance of a specific antenna system. The link budget analysis in terms of transmission, propagation, and reception is shown in Table 8.4.

The antenna along with the body were assumed to act as a transmitter, and the SNR was calculated as

$$\frac{C_1}{N_0} = P_t + G_t + L_f + G_r - N_0 = 72.45 \text{ dB/Hz} \tag{8.23}$$

TABLE 8.4 Link Budget Evaluation for Ingestible Antenna

Transmission		Propagation		Reception	
Frequency f (GHz)	1.4	Distance d (m)	2	Receiver gain G_r (dBi)	2.15
Transmitter power P_t (dB)	−57	Free-space loss L_f (dB)	41.38	Noise power density N_0 (dB/Hz)	−202.17
Transmitter Gain G_t (dBi)	−33.5				

Source: Rajagopalan (2010).

Using basic communication theory for the signal quality, the link was found to require a SNR of

$$\frac{C_2}{N_0} = \frac{E_b}{N_0} + 10\log_{10} B_r - G_c + G_d = 72.10 \text{ dB/Hz} \tag{8.24}$$

Since $C_1/N_0 > C_2/N_0$, a successful link was shown to be established between the transmitter and receiver in the scenario under investigation.

Following the same approach, three different links were compared (free-space link, in-body link where a simple dipole was used as the transmitter, and in-body link where an ingestible capsule antenna was used as the transmitter), and it was shown that, when linearly polarized antennas (dipoles) were used, the capsule link was the most robust with respect to the orientation of the transmitting antenna. A comparison of the maximum available power at the receiver from the three links for rotating transmitting antennas (Figure 8.19*a*) is shown in Figure 8.19*b*.

Lee et al. (2011) measured the received power level using a wideband spiral ingestible antenna, a circular polarized receiver antenna at a distance R, and a pig under general anesthesia. Measurements of the received power were performed inside the stomach and intestine of the pig, which are typical digestive organs. Results are shown in Figure 8.20*a*. The width (w) and gap (g) of the spiral antenna are defined in Figure 8.15*b*. When the transmitted power was 0 dBm, the received powers in the stomach and intestine were measured as −51.06 and −47.19 dBm, respectively.

If the values of the transmitted power (P_t), the received power (P_r), and the gain of the receiving antenna (G_r) are known, then the gain of the transmitting antennas (G_t) was said to be calculated with the Friis transmission equation inside a lossy medium as

$$\frac{P_r}{P_t} = \left(\frac{\lambda}{4\pi R}\right)^2 G_t G_r (e^{-\alpha R})^2 \tag{8.25}$$

where the attenuation constant is given as

$$\alpha = \text{Re}(\gamma) = \text{Re}\left(j\omega\sqrt{\mu\varepsilon}\sqrt{1 - j\frac{\sigma}{\omega\varepsilon}}\right) \tag{8.26}$$

and ε and σ are the permittivity and conductivity values of the medium at an angular frequency of ω, respectively.

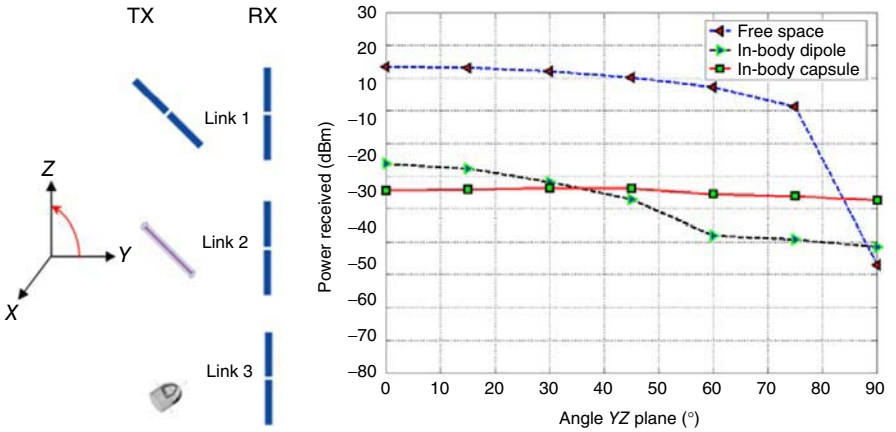

Figure 8.19 Link budget analysis for ingestible linearly polarized antennas: (*a*) orientation of antennas for three links and (*b*) comparison of the maximum power available at the receiver from the three links when the transmitting antennas rotate in the *yz* plane (Rajagopalan and Sahmat-Samii, 2010).

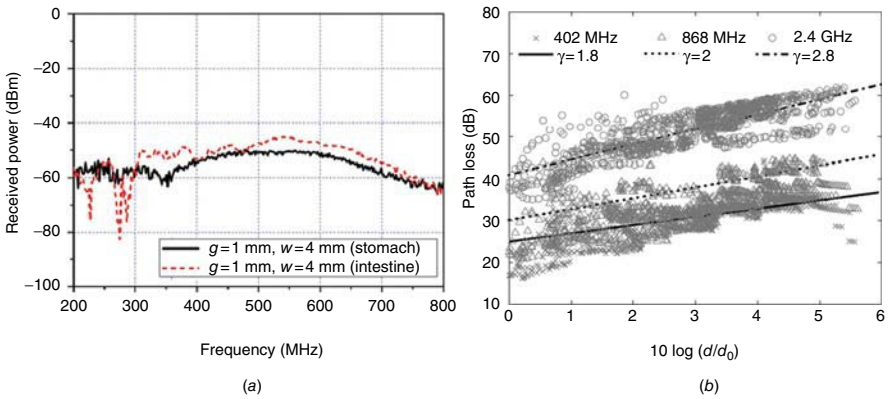

Figure 8.20 (*a*) Measured received power of a spiral ingestible antenna inside a pig (Lee et al., 2011) and (*b*) measured and empirically modeled path loss for biomedical telemetry links between ingestible antennas and receiver antennas placed in parallel to the human body (Alomainy and Hao, 2009).

Finally, biomedical telemetry radio channels from ingestible antennas at 402, 868, and 2400 MHz were numerically modeled and experimentally tested in Alomainy and Hao (2009). The aim of the study was to demonstrate a detailed analysis of wave propagation in different human tissues. The average path loss for a distance d between

TABLE 8.5 Exponent Values of Modeled Path Loss for Ingestible Antenna

Frequency (MHz)	Measured γ	Simulated γ
402	1.90	1.85
868	2.00	1.90
2400	2.80	2.60

Source: Alomainy and Hao (2009).

the transmitter and the receiver was expressed as

$$\mathrm{PL}(d) \propto \left(\frac{d}{d_0}\right)^{\gamma} \tag{8.27}$$

where γ is the path loss exponent that indicates the rate at which the path loss increases with distance, and d_0 is a reference distance (set to 10 cm in the study).

The path loss observed at any given point was said to deviate from this average value due to variations in the environment, according to a log-normal distribution. Therefore, the average path loss was represented as

$$\mathrm{PL}_{\mathrm{dB}}(d) = \mathrm{PL}_{\mathrm{dB}}(d_0) + 10\gamma \log\left(\frac{d}{d_0}\right) + X_{\sigma} \tag{8.28}$$

where X_{σ} is a zero-mean Gaussian distributed random variable with standard deviation σ.

The measurement setup included a human phantom of approximately 1.7 m in height, and an average width of 0.35 m. Animal organs (sheep liver, heart, and lungs) were used to represent human tissues. A 4 cm-long monopole without the ground plane was used as both the transmitter and the receiver, and near-field scanning was used to obtain path loss data at different distances from the body.

The exponent values of the modeled path loss based on numerical and experimental data applying empirical linear power law and least-square fitting techniques are shown in Table 8.5.

The measurement-derived exponent values were highly comparable to the numerically derived ones. Deviations may be attributed to differences in loss factors and conductivities between simulated and animal tissues. Variation of the measured path loss with distance away from the body surface is shown in Figure 8.20*b*, along with the empirically modeled path loss.

8.6 CONCLUSION AND FUTURE RESEARCH DIRECTIONS

Research performed so far in the field of design and channel modeling for on-body, implantable, and ingestible antennas is by no means exhaustive. Many more research

directions need to be considered, and further optimization of the antenna design and channel modeling procedures may be possible.

In the field of on-body antennas, further research is required on textile antennas and e-textile materials themselves before they can actually be used for reliable transmission of medical data. Treating textile antennas in the way we treat our daily garments is very demanding: washable packaging of the electronics, durable interconnections, and long-term behavior remain major challenges to be addressed. Furthermore, future designers will need to focus on multifunction and multifrequency on-body antennas.

Effort should also be directed toward ensuring that the antennas resonate and operate properly in the close vicinity of the human body, while exhibiting improved efficiency and reduced power absorption by human tissues. Metamaterials may offer the potential to reduce surface currents, thus decreasing the antenna-to-body coupling and improving the link performance of the antennas. The field of antenna diversity, that is, the use of multiple antennas at the transmitter and receiver side, will also need to be explored in an attempt to improve the speed and reliability of the on- and off-body channels.

In the field of implantable antennas, it becomes necessary to assess and quantify the trade-off between size and performance. Electrically small antennas present poor radiation performance and relatively narrow bandwidth. Design of multiband antennas, which wake up the implantable medical device when there is a need for information exchange, is also significant for conserving energy and extending the lifetime of the device. Use of efficient and accurate simulation tools and tissue models can further be considered as a key issue for the design and performance analysis of implantable antennas. The highest challenge, however, lies in experimental testing and, especially, measurements within living animals, in which careful consideration is required for developing the optimal testing protocol. Regarding the development of propagation models inside the human body, limited research has been done so far, and channel modeling has only been conducted for particular scenarios with specific antennas and orientation.

In the field of ingestible antennas, further scientific research efforts are required in determining the dependence of radiation characteristics on antenna position and orientation. Analyses presented so far provide advanced and useful information for ingestible antenna design. Nevertheless, there are still uncertainties that need to be taken into account, such as the placement of the arms, which may influence the near field, or the existence of clothing, which may affect the temperature rise. Studies regarding the wireless communication link give an insight into electromagnetic wave propagation and radiation properties of ingestible antennas; however, results are mostly given as guidelines since different human subjects exhibit different postures, body mass index, and other physiological data.

REFERENCES

Abadia K, Merli F, Zurcher JF, Mosig JR, Skrivervik AK. 2009. 3D Spiral small antenna design and realization for biomedical telemetry in the MICS band. *Radioengineering*, 18(4):359–367.

Abbasi QH, Sani A, Alomainy A, Hao Y. 2010. On-body radio channel characterization and system-level modeling for multiband OFDM ultra-wideband body-centric wireless network. *IEEE Trans. Microw. Theory Tech*., 58(12):3485–3492.

Abbasi QH, Sani A, Alomainy A, Hao Y. 2011a. Experimental characterization and statistical analysis of the pseudo-dynamic ultrawideband on-body radio channel. *IEEE Antennas Wireless Propag. Lett*., 10:748–751.

Abbasi QH, Alomainy A, Hao Y. 2011b. Characterization of MB-OFDM-based ultrawideband systems for body-centric wireless communications. *IEEE Antennas Wireless Propag. Lett.*, 10:1401–1404.

Alomainy A, Hao Y, Parini CG, Hall PS. 2005. Comparison between two different antennas for UWB on-body propagation measurements. *IEEE Antennas Wireless Propag. Lett*., 4:31–34.

Alomainy A, Hao Y, Pasveer F. 2007a. Numerical and experimental evaluation of a compact sensor antenna for healthcare devices. *IEEE Trans. Biomed. Circ. Syst*., 1(4):242–249.

Alomainy A, Hao Y, Owadally A, Parini CG, Nechayev Y, Constantinou CC, Hall PS. 2007b. Statistical analysis and performance evaluation for on-body radio propagation with microstrip patch antennas. *IEEE Trans. Antennas Propag*., 55(1):245–248.

Alomainy A, Hao Y. 2009. Modeling and characterization of biotelemetric radio channel from ingested implants considering organ contents. *IEEE Trans. Antennas Propag.*, 57:999–1005.

Alomainy A, Sani A, Rahman A, Santas JG, Hao Y. 2009. Transient characteristics of wearable antennas and radio propagation channels for ultrawideband body-centric wireless communications. *IEEE Trans. Antennas Propag.*, 57(4):875–884.

Attiya AM, Safaai-Jazi A. 2004. Simulation of ultra-wideband indoor propagation. *Microw. Opt. Technol. Lett.*, 42(2):103–108.

Balanis CA. 2002. *Antenna Theory: Analysis and Design*, 2nd ed. New York: Wiley.

Chan Y, Meng MH, Wu KL, Wang X. 2005. Experimental study of radiation efficiency from an ingested source inside a human body model. *IEEE Eng. Med. Biol. Soc*., 7754–7757.

Chen ZN. 2005. Novel bi-arm rolled monopole for UWB applications. *IEEE Trans. Antennas Propag.*, 53(2):672–677.

Chen ZN. 2007. *Antennas for Portable Devices*. New York: Wiley.

Chirwa LC, Hammond PA, Roy S, Cumming DRS. 2003a. Electromagnetic radiation from ingested sources in the human intestine between 150 MHz and 1.2 GHz. *IEEE Trans. Biomed. Eng*., 50:484–492.

Chirwa LC, Hammond PA, Roy S, Cumming DRS. 2003b. Radiation from ingested wireless devices in biomedical telemetry bands. *IEEE Electron. Lett*., 39(2):178–179.

Conway GA, Scanlon WG. 2009. Antennas for over-body-surface communication at 2.45 GHz. *IEEE Trans. Antennas Propag*., 57(4):844–855.

Conway GA, Scanlon WG, Orlenius C, Walker C. 2008. In situ measurement of UHF wearable antenna radiation efficiency using a reverberation chamber. *IEEE Antennas Wireless Propag. Lett*., 7:271–274.

Fort A, Desset C, Ryckaert J, De Doncker P, Van Biesen L, Donnay S. 2005. Ultra wide-band body area channel model. *IEEE Int Conf. Commun.*, 4:2840–2844.

Gemio J, Parron J, Soler J. 2010. Human body effects on implantable antennas for ISM bands applications: models comparison and propagation losses study. *Prog. Electrom. Res.*, 110:437–452.

Gupta SKS, Lalwani S, Prakash Y, Elsharawy E, Schwiebert L. 2003. Towards a propagation model for wireless biomedical applications. *IEEE Int. Conf. Commun*., 1993–1997.

Hall PS, Hao Y, Nechayev YI, Alomainy A, Constantinou CC, Parini C, Kamarudin MR, Salim TZ, Hee DTM, Dubrovka R, Owadally AS, Song W, Serra A, Nepa P, Gallo M, Bozzetti M. 2007. Antennas and propagation for on-body communication systems. *IEEE Antennas Propag. Mag*., 49(3):41–58.

Hertleer C, Tronquo A, Rogier H, Vallozzi L, Van Langenhove L. 2007. Aperture-coupled patch antenna for integration into wearable textile systems. *IEEE Antennas Wireless Propag. Lett*., 6:392–395.

Hu ZH, Nechayev YI, Hall PS, Constantinou CC, Hao Y. 2007. Measurements and statistical analysis of on-body channel fading at 2.45 GHz. *IEEE Antennas Wireless Propag. Lett*., 6:612–615.

Huang FJ, Lee CM, Chang CL, Chen LK, Yo TC, Luo CH. 2011. Rectenna application of miniaturized implantable antenna design for triple-band biotelemetry communication. *IEEE Trans. Antennas Propag*., 59(7):2646–2653.

Institute of Electrical and Electronics Engineers (IEEE). 1999. IEEE Standard for Safety Levels with Respect to Human Exposure to Radiofrequency Electromagnetic Fields, 3 kHz to 300 GHz, IEEE Standard C95.1-1999.

Institute of Electrical and Electronics Engineers (IEEE). 2005. IEEE Standard for Safety Levels with Respect to Human Exposure to Radiofrequency Electromagnetic Fields, 3 kHz to 300 GHz, IEEE Standard C95.1-2005.

International Commission on Non-Ionizing Radiation Protection (ICNIRP). 1998. Guidelines for limiting exposure to time–varying electric, magnetic, and electromagnetic fields (up to 300 GHz). *Health Phys.*, 74:494–522.

International Telecommunications Union—Radiocommunications (ITU-R). 1998. Recommendation ITU-R SA.1346.

Jovanov E, O'Donnell-Lords A, Raskovic D, Cox P, Adhami R, Andrasik F. 2003. Stress monitoring using a distributed wireless intelligent sensor system. *IEEE Eng. Med. Biol. Mag*., 22(3):49–55.

Karacolak T, Cooper R, Topsakal E. 2009. Electrical properties of rat skin and design of implantable antennas for medical wireless telemetry. *IEEE Trans. Antennas Propag*., 57(9):2806–2812.

Karacolak T, Cooper R, Butler J, Fisher S, Topsakal E. 2010. In vivo verification of implantable antennas using rats as model animals. *IEEE Antennas Wireless Propag. Lett*., 9:334–337.

Karacolak T, Hood AZ, Topsakal E. 2008. Design of a dual-band implantable antenna and development of skin mimicking gels for continuous glucose monitoring. *IEEE Trans. Microw. Theory Techn*., 56(4):1001–1008.

Kawoos U, Tofighi MR, Warty R, Kralick FA, Rosen A. 2008. In-vitro and in-vivo trans-scalp evaluation of an intracranial pressure implant at 2.4 GHz. *IEEE Trans. Microw. Theory Tech*., 56(10):2356–2365.

Khan I, Hall PS. 2009. Multiple antenna reception at 5.8 and 10 GHz for body-centric wireless communication channels. *IEEE Trans. Antennas Propag*., 57(1):248–255.

Khan I, Hall PS, Serra AA, Guraliuc AR, Nepa P. 2009. Diversity performance analysis for on-body communication channels at 2.45 GHz. *IEEE Trans. Antennas Propag.*, 57(4):956–963.

Kim J, Rahmat-Samii Y. 2004. Implanted antennas inside a human body: Simulations, designs, and characterizations. *IEEE Trans. Microw. Theory Techn*., 52(8):1934–1943.

Kim J, Rahmat-Samii Y. 2006. SAR reduction of implanted planar inverted F antennas with non–uniform width radiator. *IEEE Int. Symp. Antennas Propag*., 1091–1094

Kiourti A, Christopoulou M, Nikita KS. 2011. Performance of a novel miniature antenna implanted in the human head for wireless biotelemetry. *IEEE Int. Symp. Antennas Propag.*, Spokane, Washington, pp. 392–395.

Kiourti A, Nikita KS. 2011. Meandered versus spiral novel miniature PIFAs implanted in the human head: Tuning and performance. 2nd ICST Int. Conf. Wireless Mobile Commun. Healthcare, Kos Island, Greece, pp. 80–87.

Kiourti A, Nikita KS. 2012a. A review of implantable patch antennas for biomedical telemetry: Challenges and Solutions. *IEEE Antennas Propag. Mag.*, 54(3):210–228.

Kiourti A, Nikita KS. 2012b. Miniature scalp-implantable antennas for telemetry in the MICS and ISM bands: Design, safety considerations and link budget analysis. *IEEE Trans. Antennas Propag*., 60(6):3568–3575.

Kiourti A, Nikita KS. 2012c. Accelerated design of optimized implantable antennas for medical telemetry. *IEEE Antennas Wireless Propag. Lett*., 11:1655–1658.

Kiourti A, Nikita KS. 2012d. Recent advances in implantable antennas for medical telemetry. *IEEE Antennas Propag. Mag*., 54(6):190–199.

Kiourti A, Nikita KS. 2013. Design of implantable antennas for medical telemetry: Dependence upon operation frequency, tissue anatomy and implantation site. *Int. J. Monit. Surv. Technol.*, 1(1):16–33.

Kiourti A, Psathas KA, Costa JR, Fernandes CA, Nikita KS. 2013. Dual-band implantable antennas for medical telemetry: A fast design methodology and validation for intra-cranial pressure monitoring. *Prog. Electrom. Res.*, 141:161–183.

Klemm M, Locher I, Tröster G. 2004. A novel circularly polarized textile antenna for wearable applications. 7th Europ Microw Week, Amsterdam, The Netherlands, pp. 137–140.

Lee CM, Yo TC, Huang FJ, Luo CH. 2009. Bandwidth enhancement of planar inverted–F antenna for implantable biotelemetry. *Microw. Opt. Technol. Lett.*, 51(3):749–752.

Lee SH, Lee J, Yoon YJ, Park S, Cheon C, Kim K, Nam S. 2011. A wideband spiral antenna for ingestible capsule endoscope systems: Experimental results in a human phantom and a pig. *IEEE Trans. Biomed. Eng.*, 58(6):1734–1741.

Liu WC, Chen SH, Wu CM. 2008. Implantable broadband circular stacked PIFA antenna for biotelemetry communication. *J. Electromagn. Waves Appl.*, 22:1791–1800.

Liu WC, Chen SH, Wu CM. 2009. Bandwidth enhancement and size reduction of an implantable PIFA antenna for biotelemetry devices. *Microw. Opt. Technol. Lett.*, 51(3):755–757.

Okoniewski M, Stuchly MA. 1996. A study of the handset antenna and human body interaction. *IEEE Trans. Microw. Theory Tech.*, 44(10):1855–1864.

Osman MAR, Rahim MKA, Samsuri NA, Salim HAM, Ali MF. 2011. Embroidered fully textile wearable antenna for medical monitoring applications. *Prog. Electrom. Res.*, 117:321–337.

Rajagopalan H, Rahmat-Samii Y. 2010. Link budget analysis and characterization for ingestible capsule antenna. *Int. Workshop Antenna Technol.*, pp. 1–4.

Rucker D, Al-Alawi A, Adada R, Al-Rizzo HM. 2007. A miniaturized tunable microstrip antenna for wireless communications with implanted medical devices. ICST 2nd Int Conf on Body Area Networks, Brussels, Belgium, pp. 1–4.

Salonen PO, Yang F, Rahmat-Samii Y, Kivikoski M. 2004a. WEBGA-Wearable electromagnetic band-gap antenna. *IEEE Antennas Propag. Int. Symp.*, 1:451–454.

Salonen P, Rahmat-Samii Y, Hurme H, Kivikoski M. 2004b. Dual band wearable textile antenna. IEEE Antennas Propag. *Soc. Int. Symp.*, pp. 463–466.

Sani A, Alomainy A, Hao Y. 2009. Numerical characterization and link budget evaluation of wireless implants considering different digital human phantoms. *IEEE Trans. Microw. Theory Tech.*, 57(10):2605–2613.

Sani A, Rajab M, Foster R, Hao Y. 2010. Antennas and propagation of implanted RFIDs for pervasive healthcare applications. *Proc. IEEE*, 98(9):1648–1655.

Scanlon WG, Evans NE. 2001. Numerical analysis of bodyworn UHF antenna systems. *IEE Electron Commun. Eng. J.*, 13(2):53–64.

Serra AA, Nepa P, Manara G, Hall PS. 2007. Diversity measurements for on-body communication systems. *IEEE Antenna Wireless Propag. Lett.*, 6(1):361–363.

Skrivervik AK, Merli F. 2011. Design strategies for implantable antennas. Antennas Propag Conf, pp. 1–5.

Soontornpipit P, Furse CM, Chung YC. 2004. Design of implantable microstrip antenna for communication with medical implants. *IEEE Trans. Microw. Theory Tech.*, 52:1944–1951.

Soontornpipit P, Furse CM, Chung YC. 2005. Miniaturized biocompatible microstrip antenna using genetic algorithm. *IEEE Trans. Antennas Propag.*, 53(6):1939–1945.

Tronquo A, Rogier H, Hertleer C, Van Langenhove L. 2006. A robust planar textile antenna for wireless body lans operating in the 2.45-GHz ISM band. *Inst. Elect. Eng. Electron. Lett*., 42(3):142–143.

Valdastri P, Menciassi A, Arena A, Caccamo C, Dario P. 2004. An implantable telemetry platform system for in vivo monitoring of physiological parameters. *IEEE Trans. Inf. Technol. Biomed.*, 8(3):271–278.

Wang Q, Wang J. 2009. Performance of on-body chest-to-waist UWB communication link. *IEEE Microw. Wireless Compon. Lett.*, 19(2):119–121.

Warty R, Tofighi MR, Kawoos U, Rosen A. 2008. Characterization of implantable antennas for intracranial pressure monitoring: Reflection by and transmission through a scalp phantom. *IEEE Trans. Microw. Theory Tech.*, 56(10):2366–2376.

Weiss MD, Smith JL, Bach J. 2009. RF coupling in a 433 MHz biotelemetry system for an artificial hip. *IEEE Antennas Wireless Propag. Lett.*, 8:916–919.

Wong KL, Lin CI. 2005. Characteristics of a 2.4-GHz compact shorted patch antenna in close proximity to a lossy medium. *Microw. Opt. Technol. Lett*., 45(6):480–483.

Xia W, Saito K, Takahashi M, Ito K. 2009. Performances of an implanted cavity slot antenna embedded in the human arm. *IEEE Trans. Antennas Propag.*, 57(4):894–899.

Xie X, Li G, Chen XK, Li XW, Chi BY, Han SG. 2004. A novel low power IC design for bi-directional digital wireless endoscopy capsule system. IEEE Int. Workshop Biomed. Circuit. Syst., pp. S1.8-5–1.8-8.

Xu L, Max QH, Ren HL. 2008a. Electromagnetic radiation from ingested sources in the human intestine at the frequency of 2.4 GHz. Progress Electrom. Res. Symp., pp. 893–897.

Xu L, Maz MQH, Ren H, Chan Y. 2008b. Radiation characteristics of ingested wireless device at frequencies from 430 MHz to 3 GHz. IEEE Conf. Eng. Med. Biol. Soc., pp. 1250–1253.

Xu L, Meng MQH, Chan Y. 2009a. Effects of dielectric parameters of human body on radiation characteristics of ingestible wireless device at operating frequency of 430 MHz. *IEEE Trans. Biomed. Eng.*, 56:2083–2094.

Xu L, Meng MQH, Ren H, Chan Y. 2009b. Radiation characteristics of ingestible wireless devices in human intestine following radio frequency exposure at 430, 800, 1200, and 2400 MHz. *IEEE Trans Antennas Propag.*, 57:2418–2428.

Zasowski T, Althaus F, Stager M, Wittneben A, Troster G. 2003. UWB for noninvasive wireless body area networks: Channel measurements and results. IEEE Conf. UWB Syst. Technol., Reston, VA, pp. 285–289.

Zhao Y, Hao Y, Alomainy A, Parini C. 2006. UWB on-body radio channel modeling using ray theory and sub-band FDTD method. *IEEE Trans. Microw. Theory Tech.*, 1–9.

Zhu S, Langley R. 2009. Dual-band wearable textile antenna on an EBG substrate. *IEEE Trans. Antennas Propag.*, 57(4):926–935.